Probing the role of the so-called inactive transition metal in conversion reactions : not so inactive!

Karen E. Johnston,[1,2,3*] Ali Darwiche,[4,5] Lorenzo Stievano,[3,4,5] Kent J. Griffith,[2] Nicolas Dupré,[5,6*] Clare P. Grey[2] and Laure Monconduit[3,4,5]

[1]Department of Chemistry, Durham University, Durham, DH1 3LE

[2]Department of Chemistry, University of Cambridge, Lensfield Road, Cambridge,
CB2 1EW, United Kingdom

[3]ALISTORE Alistore-ERI, CNRS FR, Amiens 3104, France

[4] ICGM, Univ. Montpellier, CNRS, ENSCM, Montpellier, France,

[5]Réseau sur le Stockage Electrochimique de l'Energie (RS2E), FR CNRS 3459, France

[6] Nantes Université, CNRS, Institut des Matériaux de Nantes Jean Rouxel, IMN,
Nantes F-44000, France

Abstract

Ternary alloys such as TiSnSb and NbSnNb have been proposed as suitable negative electrode materials for lithium-ion batteries due to their large capacities and rate capability over many cycles. During lithiation, TiSnSb undergoes a conversion reaction, leading to the formation of multiple, highly reactive species. Previous *in situ* ^{119}Sn Mössbauer and ^{7}Li magic-angle spinning (MAS) NMR spectroscopic studies suggested the phases Li_3Sb, Li_7Sn_2, Li_7Sn_3 and $Li_{2-x}Sb$ are formed at the end of lithiation alongside Ti or Nb nanoparticles. However, their stability and overall contribution to the conversion reaction is not yet fully understood. A series of model Sn- and Sb-based mixtures and alloys (both binary and ternary) have been investigated at the end of lithiation using ^{7}Li MAS NMR spectroscopy to determine both the phases formed and their contribution to the conversion reaction. In all cases, a mixture of reactive lithiated phases and metallic nanoparticles are formed at the end of lithiation. Changing the nature of the inactive element in binary and ternary alloys changes the local Li environment and the observed chemical shifts. Considerable differences in chemical shift are observed for alloys relative to less intimate mixtures. The synthetic conditions used, particularly the intimacy of mixing achieved during synthesis, is key in determining both the phases formed and how the reaction proceeds, *i.e.*, via a conversion or alloying reaction. The data presented show that the so-called “inactive” element and its nature in fact plays a key role in the conversion mechanism and therefore influences the ability for this class of materials to be commercialised in the future.

Introduction

Lithium rechargeable batteries are considered the technology of choice for many devices and applications, including portable electronics and zero emission vehicles [1,2]. However, with increasing usage comes the demand for better performance, *i.e.*, materials with higher energy densities.

Metallic Sb and Sn offer theoretical capacities that are double (660 mA·h/g for Li_3Sb) and triple (991 mA·h/g for $Li_{22}Sn_5$) that of the current commercial anode material graphite, making them promising negative electrode materials [3]. However, a major drawback of using metallic Sb or Sn electrodes is the severe volume expansion exhibited during Li^+ insertion. One solution to this problem is the use of intermetallic composites, *e.g.*, Sb-X, where X is a transition metal (Fe, Co, Ni, Cu and Mn). Upon lithiation, Sb reacts with lithium to form a Li-Sb alloy, while the transition metal acts as an inactive matrix to buffer the volume change and maintain the cyclability of the electrode. Some binary and ternary Sb-based alloys are known to exhibit high energy densities and long cycle lives, including $NiSb_2$, $TiSb_2$, NbSnSb and TiSnSb [4-8]. However, complete mechanisms for lithium insertion and removal are currently unknown. Specifically, the role of the transition metal in the conversion reaction is not fully understood. Elucidating such mechanisms is essential if we want to design better negative electrodes, and to do this, studies of model systems such as Li-Sb and Li-Sn are needed.

Weppner and Huggins initially studied the thermodynamic properties of Li-Sb using the galvanic cell coulometric titration technique and discovered a limited solid solution existed for Li_3Sb, from $Li_{2.9985}Sb$ to $Li_{3.006}Sb$ at 360 °C [9]. The corresponding phase diagram (published later) identified the phases Li_2Sb and Li_3Sb [10]. Several studies have since determined the electrochemical reactions occurring [11, 12]. The most recent of which used *in situ* X-ray diffraction (XRD) methods and found that, upon delithiation, a two phase region of Li_3Sb and Sb is formed, with no Li_2Sb detected [12]. In contrast, during lithiation, a two-step reaction occurs with the formation of Li_2Sb followed by Li_3Sb, as described by the following reactions:

$$2\ \mathrm{Li} + \mathrm{Sb} \rightarrow \mathrm{Li_2Sb} \quad (1)$$

and

$$\mathrm{Li} + \mathrm{Li_2Sb} \rightarrow \mathrm{Li_3Sb} \quad (2)$$

A combined theoretical and experimental study by Chang *et al.* [13] discovered that both Li_2Sb and Li_3Sb can tolerate some degree of off-stoichiometry and a non-stoichiometric phase of Li_2Sb, $Li_{2-x}Sb$, was identified.

The Li-Sn system has been studied extensively and the phase diagram is relatively well understood, with seven known Li-Sn phases: LiSn, Li_2Sn_5, Li_5Sn_2, Li_7Sn_2, Li_7Sn_3, $Li_{13}Sn_5$, and $Li_{22}Sn_5$ [14], all of which have been characterized via XRD and ^{119}Sn Mössbauer spectroscopy [15-23].

The ternary alloy TiSnSb has been proposed as a suitable negative electrode material in Li-ion batteries. TiSnSb is known to undergo a conversion reaction, leading to a reversible capacity of 540 mA·h/g at a rate of 2C (2 Li per formula unit in 1 hr) [5]. However, at present, the precise mechanism by which the conversion reaction occurs is unclear. Using *operando* XRD and ^{119}Sn Mössbauer studies it was determined that, during the first lithiation, TiSnSb undergoes a conversion process leading to the simultaneous formation of Li_3Sb and Li_7Sn_2 [5]. The following, albeit simplified, electrochemical equation was proposed for Li insertion:

$$\mathrm{TiSnSb} + 6.5\ \mathrm{Li} \rightarrow \mathrm{Ti} + \mathrm{Li_3Sb} + 0.5\ \mathrm{Li_7Sn_2} \qquad (3)$$

A study of TiSnSb that combined ^{7}Li magic-angle spinning (MAS) NMR with ^{119}Sn Mössbauer spectroscopy determined that at least four distinct phases are formed at the end of lithiation, believed to be Li_3Sb, Li_7Sn_2, Li_7Sn_3 and $Li_{2-x}Sb$ [24]. The corresponding delithiation mechanism is likely to involve the formation of a ternary alloy close to TiSnSb. Using X-ray absorption near edge structure spectroscopy (XANES), Fehse *et al.* demonstrated the formation of Ti nanoparticles upon lithiation and determined that the Ti−Sn−Sb species formed after one complete lithiation/delithiation cycle is distinct from the starting material TiSnSb [25]. However, the precise mechanism and structure, as well as the influence of the so-called inactive element (here Ti), remain elusive. Amorphous Li-Sn alloys are also beyond the detection capabilities of XRD and, in such cases, techniques capable of probing the short-range order of a material are required. NMR and X-ray absorption spectroscopies (XAS) can detect the local structure among long-range disorder and are therefore ideal probes of such systems.

To assist in confirming the phases formed at the end of lithiation of TiSnSb and to elucidate the influence of the various metallic elements, *i.e.*, whether they are alloying with lithium or considered inactive, we have chosen to investigate the lithiation of a series of model Sb- and Sn-based compounds via ^{7}Li NMR and XAS spectroscopy. The first part of this paper briefly describes the electrochemical performance of TiSnSb and the ^{7}Li NMR data obtained at the end of lithiation are presented, before then focusing on samples of Li_2Sb and Li_3Sb prepared via ball milling and electrochemical methods and analysis of their corresponding ^{7}Li NMR spectra with respect to the Li local environments. Finally, the lithiation of several Sb- and Sn-based model compounds (including Sb, Sn, SnSb, $TiSb_2$, $NbSb_2$, TiSnSb, NbSnSb, mixtures of SnSb and TiSnSb and the series $Ti_{1-y}Nb_ySnSb$, where $y = 0.25$, 0.5 and 0.75) are investigated and their corresponding ^{7}Li NMR data presented.

The results obtained provide detailed insight into the phases formed during the conversion reaction and their relative stabilities, as well as the influence of the active (Sn, Sb) and so-called inactive elements (Ti, Nb) on the local lithium environments formed at the end of the lithiation process. These lithiated phases and local environments were previously found to be highly reactive and unstable. This instability is extremely important, as it is believed to play a key role in the conversion mechanism, and the associated performance. The cause of such phase instabilities is, however, currently unknown. To understand this phenomenon and its contribution to the conversion reaction, studies of model Ti, Sn and Sb-based systems are required. Moreover, the approach developed in the present work provides valuable insight into this complex family of materials and enables a deeper understanding of the conversion mechanism to be gained.

Experimental

Sample Preparation. All samples were synthesized by mechanical milling of the appropriate elemental powders (*e.g.*, Ti, Sn, Sb, Nb, V) under an Ar atmosphere using a SPEX 8000 ball mill. All elemental powders were obtained from commercial sources (>99.9 %). In all cases, 1 g of metallic powder was used in a 45 ml grinding jar with 6 balls (5 g each). Both the jar and the balls were made of hardened stainless steel. Active milling times were: Li_2Sb and Li_3Sb = 2×100 min, TiSnSb = 5×100 min, SnSb = 1×100 min, $TiSb_2$ = 3×100 min, $NbSb_2$ = 5×100 min and NbSnSb = 5×100 min. Mixtures of SnSb and TiSnSb were prepared by manual grinding of the Ti, Sn and Sb powders in a mortar and pestle. For clarity, these mixtures are referred to as M1 (Sn+Sb) and M3 (Ti+Sn+Sb) throughout the manuscript. An additional mixture of SnSb was prepared using a combination of manual grinding and 5 minutes of ball milling. This is referred to as M2 (Sn+Sb ball mill). Samples in the series $Ti_{1-y}Nb_ySnSb$ were synthesized under an Ar atmosphere using a Planetary Ball Mill PM 100. An active milling time of 28 hr (500 rpm) was used.

X-ray Diffraction. The crystalline purity of each sample was determined via X-ray diffraction. All diffraction patterns were recorded for $2\theta = 10 – 90°$ using an X'pert diffractometer equipped with Cu K_α radiation.

Electrode Preparation. To prepare electrodes, carboxymethyl cellulose (CMC) (degree of substitution DS = 0.7, and viscosity average molecular weight M_w = 250,000 g mol^{-1}, Aldrich) was used as a binder with two conductive additives: (i) vapor-grown carbon fibers (VGCF, diameter 100-200 nm and length 10-20 µm, Brunauer-Emmett-Teller (BET) surface area 15 m^2 g^{-1}, SHOWA DENKO) and (ii) carbon black Y50A (CB, BET primary particle size 20-60 nm, primary aggregate size 100 nm, 70 m^2 g^{-1}). The active materials, CMC, and additives were manually ground in a mortar and pestle with a weight ratio of 70/12/9/9% (Active Material/CMC/Y50A/VGCF). The mixture was mixed with deionised water in a silicon nitride vial containing three 9.5 mm diameter silicon nitride balls. A Fritsch Pulverisette 7 was used to ball mill the mixture at 500 rpm for 1 hour. The slurry was tape cast onto 22 μm thick copper foil at 150 μm thickness. The electrodes were dried for 12 h at room temperature and at 100 °C for 1 h under vacuum.

Electrochemical Tests. All electrodes were cycled against Li metal with $LiPF_6$ 1 M in EC:DMC using conventional two-electrode Swagelok™ cells. Each cell was assembled inside an argon-filled glovebox. Electrochemical lithiation curves were recorded on a multi-channel VMP system under galvanostatic conditions at rates of C/2 (1 Li per formula unit in 2 h) and 4C down to 10 mV vs. Li^+/Li. The cells were then disassembled in a glovebox, where the active materials were extracted, rinsed with dimethyl carbonate (DMC), dried and packed into 2.5 mm zirconia rotors for NMR analysis.

X-ray Absorption Spectroscopy. XAS measurements were carried out on beamline XAFS (Elettra, Trieste, Italy). Ti K-edge spectra were recorded in transmission mode in the range 4800-6100 eV. Fourier transformations were performed using k-weighting and the structural parameters were determined by curve fitting procedures using the IFEFFIT software suite [26] on the basis of the published crystal structure of TiSnSb [27]. The pristine material was measured as a self-supported CMC-based electrode film of the appropriate thickness. The film was prepared using the method described above and contained ~3 mg/cm^2 of TiSnSb. Spectra of the material after full lithiation and the following full delithiation were measured with the self-supported electrode film mounted in a customised *in situ* cell with a sturdy stainless steel body and beryllium window as both the closure and the current collector [28]. A solution of 1 M $LiPF_6$ in EC:PC:3DMC and Celgard were used as the electrolyte and separator, respectively. The two spectra were measured at the end of the respective processes under OCV conditions and without allowing the sample to relax.

Solid-State NMR Spectroscopy. All room temperature ^{7}Li ($I = 3/2$) magic-angle spinning (MAS) NMR spectra were acquired using a Bruker Avance 200 MHz spectrometer, equipped with a wide-bore 4.7 T magnet using a Larmor frequency of 77.87 MHz. The powdered samples were packed into conventional 2.5 mm zirconia rotors and a MAS rate of 25 kHz was employed. ^{7}Li chemical shifts were referenced to 1 M LiCl (aq) at $\delta_{iso} = 0.0$ ppm. In order to eliminate signal corresponding to the probe, ^{7}Li MAS NMR spectra were acquired using a Hahn echo ($90 - \tau - 180 - \tau$) pulse sequence. Optimized recycle intervals were 30 s. Spectral analysis and fitting were performed within the Dmfit software package [29].

Results and Discussion

TiSnSb

The ternary alloy TiSnSb is a complex system that has been studied extensively in recent years using techniques such as *in situ* XRD, *operando* ^{119}Sn Mössbauer spectroscopy and ^{7}Li MAS NMR spectroscopy. TiSnSb is known to undergo a conversion reaction, resulting in the formation of multiple lithiated phases at the end of lithiation. Using *in situ* ^{119}Sn Mössbauer spectroscopy, the lithiated tin species obtained at the end of lithiation are known to have an average composition close to Li_7Sn_2 [24].

A sample of TiSnSb was lithiated to a cut-off potential of 10 mV at a rate of C/2. The corresponding electrochemical profile is shown as an inset in Figure 1. During lithiation, a rapid decrease in potential from an open circuit voltage (OCV) of 1.4 V to 0.6 V is observed, assigned to formation of the solid-electrolyte interphase (SEI). This is followed by a redox process around 0.3 V. As in all conversion type materials, TiSnSb undergoes a specific low voltage first lithiation. The voltage profile exhibits a progressive decrease and is characteristic of the ternary alloy TiSnSb [5, 24]. No distinct or separate processes are observed for the lithiation of tin or antimony, as in the case of SnSb [30, 31]. At the end of lithiation, approximately 8 Li per formula unit are inserted into the TiSnSb structure, in good agreement with previous findings [5, 24].

At the end of lithiation, the cell was stopped, disassembled and the active materials were extracted, rinsed and dried prior to acquisition of the ^{7}Li MAS NMR spectrum, shown in Figure 1. Based on previous studies of Sb and TiSnSb, peaks at 2.3, 3.5 and 8.5 ppm have been assigned to the SEI, Li_3Sb and Li_7Sn_2, respectively, whilst the second group of resonances at ~19.5 and 22 ppm are assigned to Li_7Sn_3 and $Li_{2-x}Sb$, respectively [24]. In previous work, the phases formed at the end of lithiation were identified as being highly reactive and unstable. Furthermore, a strong contribution from the SEI, estimated at approximately 20% of the total integrated intensity is present. Such a strong contribution is consistent with previous work by our group [32] and is explained by the significant irreversible capacity corresponding to the SEI formation during the first cycle of TiSnSb (on the order of 24% of the total capacity for the first reduction). The typical electrochemical behavior of TiSnSb upon extended cycling is also detailed in reference 32. The signal assigned to the SEI contains individual contributions from the different lithiated species that form the SEI (polyalkyl carbonate species such as polymeric chains containing $–OCO_2Li$ groups, $ROCO_2Li$, $(CH_2OCO_2Li)_2$ as well as other byproducts coming from the degradation of the $LiPF_6$ salt such as LiF). Nevertheless, considering the narrow chemical shift range for diamagnetic lithiated species and the strong overlap with Li-Sb and Li-Sn environments, it is not possible to fully discriminate them and their exact contribution.

The chemical shifts for all phases and local Li environments discussed here are detailed in Table 1. The instability of the phases formed at the end of lithiation is extremely important as it is believed to play a key role in the conversion mechanism. The cause of such phase instabilities is, however, currently unknown. To understand this phenomenon and their contribution to the conversion reaction, studies of model Ti, Sn and Sb-based systems are required. This will provide valuable insight into the precise role of each element in the TiSnSb system.

Table 1: Various compounds and local Li environments discussed in the current study with their method of preparation, ^{7}Li MAS NMR observed shift and corresponding reference. In the case of electrodes, ^{7}Li NMR shifts are given only for electrodes cycled at C/2.

Compound	**Preparation**	**^{7}Li Chemical shift (ppm)**	**Comments**	**Reference**
Li_2Sb	mechanosynthesis	0.8	-	This work
	electrochemical	40 and −17	Possibly non stoichiometric	13
Li_3Sb « bulk »/ « isolated »	mechanosynthesis	−7 to −8.5	-	This work, 13*
	Sb electrodes	−8.8, −8.2*	-	This work, 13*
	Sn, Sb, Ti mixtures	−8	No influence of the inactive element	This work
Li_3Sb surface defective/strong interaction with surrounding metallic nanoparticles	Sb electrode	3.8, −1.4*, 3.2, −7		13*, this work
	SnSb electrodes	−3.3, −4.8	At the end of lithiation, when both Sn and Sb are fully lithiated (no Sn metallic particle remain)	30, this work
	TiSnSb electrodes	3.5	Influence of the nature of the inactive element	This work, 24
	$TiSb_2$ electrodes	10.8, 11.9		This work
	$NbSb_2$ electrodes	7.8		This work
	NbSnSb electrodes	1.4		This work
Li_7Sn_2	Mechanosynthesis or electrochemical	8.5	No influence of the preparation method. No influence of the inactive element in Ti- and Nb-based alloys	24, 33
Li_7Sn_3		16 to 19		24, 33
LiSn		32 to 42		33, this work
$Li_{22}Sn_5$		78		33
$Li_{13}Sn_5$		32		33

* Ref. 13 likely inverted the attribution of −8.5 and 3.8 ppm resonances to stoichiometric and non-stoichiometric Li_3Sb.

X-ray Absorption Spectroscopy

Ti K-edge X-ray absorption spectroscopy was used to follow the speciation of titanium during lithiation and the following delithiation of TiSnSb. The corresponding results are detailed in Supporting Information. In summary, the strong increase in the intensity of the Ti-Ti contribution, together with a decrease in the Ti-Sn(Sb) contribution, is in line with the transformation of pristine TiSnSb into Ti-rich metal nanoparticles, probably surrounded by a Sn(Sb) rich environment. The observed increase in the Ti-Ti bond length, that moves towards the value usually observed for bulk Ti metal (2.87 Å), is further confirmation of the formation of Ti metal nanoparticles at the end of the lithiation of the active material.

The spectrum of the delithiated electrode is very similar to that of the initial material, suggesting that delithiation produces a material that is chemically similar to pristince TiSnSb. A slight, but significant, decrease of the Ti-Sn(Sb) bond length is observed (Table S1), together with a small increase of the Debye-Waller factors, in line with a decrease in the crystallinity of the material. These results are consistent with the previous study by Fehse *et al*. and confirm a similar behaviour of TiSnSb [25].

Model Systems

Li_2Sb and Li_3Sb – mechanical synthesis

There are two known lithiated phases of Sb; Li_2Sb and Li_3Sb [13]. Li_2Sb can be described using the Zintl-Klemm concept. It is composed of an undistorted, infinite linear [$\ldots Sb^{2-}\ldots$] chain and one distorted linear chain with [Sb^{2-} Sb^{2-}] dumbbells (Figure S3(a)) with two crystallographically distinct Li sites. Li_3Sb has a single isolated Sb^{3-} site and two crystallographically distinct Li sites, one octahedral and one tetrahedral (Figure S3(b)).

Samples of Li_2Sb and Li_3Sb were synthesized via ball milling. The structure and phase purity of each sample was verified using XRD. The sample of Li_2Sb was in agreement with the hexagonal phase (space group P-62m) and Li_3Sb agreed with the cubic phase (space group Fm-3m). The ^7Li MAS NMR spectra obtained for Li_2Sb and Li_3Sb are shown in Figures 2(a) and (b), respectively. Chemical shifts for all phases and Li local environments discussed in this article are detailed in Table 1. The ^7Li NMR spectrum obtained for Li_2Sb displays a single broad resonance centred at 0.8 ppm. In contrast, the ^7Li NMR spectrum acquired for Li_3Sb displays two distinct resonances centred at −8.49 and 0.8 ppm, respectively. The resonance at 0.8 ppm is believed to be a small impurity of Li_2Sb. Hence, in both cases, only a single resonance is observed, suggesting the presence of a single Li site in each. This is in contrast to the XRD data and the reported crystal structures, where two distinct Li environments are reported for each. Hence, using ^7Li NMR, it is not possible to distinguish the different Li sites.

Li_2Sb and Li_3Sb – Electrochemical lithiation of Sb

Sb electrodes were lithiated to a cut-off potential of 10 mV at rates of C/2 and 4C. The corresponding electrochemical profiles are shown as insets in Figures 2(c) and (d). After reaching the end of lithiation each cell was stopped, disassembled and the active materials were extracted, rinsed and dried prior to acquisition of the ^{7}Li NMR spectra (Figures 2(c) and (d)). In both cases, two distinct resonances are observed, centred at −8.8 ppm and 0 ppm. Based on the spectra obtained for the ball milled samples of Li_2Sb and Li_3Sb, these are assigned to Li_3Sb and the SEI, respectively. It is possible there is a small contribution from Li_2Sb beneath the resonance at 0 ppm. Based on previous literature, there could be a small amount of Li_2Sb formed at the end of lithiation due to the two-step reaction occurring [12], however, Li_3Sb is expected to be the main phase at the end of lithiation [11]. Also shown in Figures 2(c) and (d) are the ^{7}Li NMR spectra obtained after a relaxation period. In both cases, very little evolution occurs, suggesting the Li_3Sb produced via electrochemical methods is stable. However, it is noted that two additional features are observed at 40 and −17 ppm in the spectrum acquired after a relaxation period (Figure 2(d)). Previous *ex situ* ^{7}Li MAS NMR studies of lithiated Sb attributed these resonances to Li_2Sb [13]. This is in contrast to the data presented above for the ball milled sample of Li_2Sb, where a single resonance was observed at 0.8 ppm. The presence of Li_2Sb after a relaxation period is interesting as previous XRD studies suggested only Li_3Sb to be present at the end of lithiation. This suggests that the Li_3Sb formed at the end of lithiation is somewhat reactive and can undergo structural rearrangement to form Li_2Sb. The study by Chang *et al*. suggested Li_2Sb and Li_3Sb can tolerate some degree of non-stoichiometry [13]. However, the transformation between phases was not investigated. It is possible that structural rearrangements between Li_2Sb and Li_3Sb are induced by the presence of non-stoichiometric phases or vacancies in the structures. However, this is beyond the scope of the current study.

In a study of TiSnSb using ^{7}Li MAS NMR, the phase Li_3Sb (formed during the conversion reaction) was assigned to the resonance at 3.5 ppm observed at the end of lithiation, based on previous *in situ* XRD and *ex situ* ^{7}Li MAS NMR studies [13, 24]. However, this appears to be in contrast to the ^{7}Li NMR data obtained for the Li_3Sb obtained through mechanosynthesis. Here, when the phase Li_3Sb is obtained in isolation a negative chemical shift is consistently observed, irrespective of the synthetic method, *i.e.*, ball milled vs. electrochemical. This suggests that either one of the assignments is incorrect or the two individual assignments are correct but in the case of the TiSnSb study there is an additional influence on the observed chemical shift, likely caused by the nearby metallic particles and their effect on the electronic properties. Fernández-Madrigal *et al.*, recently investigated the interaction of Li with Sb in SnSb electodes via ^{7}Li MAS NMR and observed resonances at negative chemical shifts, −3.3 and −4.8 ppm at 0.58 V. These resonances were assigned to Li_xSb with x close to 3, thus most probably non-stoichiometric considering the relatively high potential of the cut-off during lithiation. In addition, at this stage, full lithiation of the electrode is not yet complete and some Sn metallic particles remain. Similarly, between 0.42 and 0.3 V, where Sn metallic particles are expected to remain, only resonances exhibiting positive NMR shifts (between 0 and 10 ppm) were observed. Only when reaching the full lithiation of the electrode, *e.g.*, Sb and Sn are fully alloyed with Li, some resonances with negative shifts are observed again, in which a Knight shift, due to a close interaction with surrounding/dilute metallic Sn particles, is not or less present [30]. Although the ^{7}Li NMR data presented above (*vide supra*), where it is not possible to distinguish between the two Li environments are in contrast with the work of Madrigal *et al.* [30], the presence of resonances at negative chemical shift is in good agreement with the present study.

In the study by Chang *et al*. [13], Sb electrodes were cycled at a very slow rate, C/30 (corresponding to a full lithiation in 30 hours). This is considerably slower than the rate used during both the current study and the recent study of TiSnSb. Different stages of lithiation were studied by Chang *et al*. and the depth of lithiation was found to have a substantial influence on the ^{7}Li chemical shift. For example, non-stoichiometric phases of Li_3Sb, $Li_{3-\zeta}Sb$, were observed at shifts between −1.4 and −8.2 ppm, whilst stoichiometric Li_3Sb was reported at 3.8 ppm. It is, however, noted that in the study by Chang *et al*. the Sb electrodes were not rinsed prior to NMR analysis. The presence of decomposition products and/or residual electrolyte can influence the local lithium environments and, hence, the chemical shift. Hence, the post cycling treatment of the electrodes may also have an effect on the phases formed. We tentatively suggest that their assignment was not correct, the −8.2 ppm shift being consistent with bulk/isolated/stoichiometric Li_3Sb while less negative (−1.4 ppm) and positive (3.8 ppm) shifts seem more in line with the Li local environment in Li_3Sb being subjected to a modification or external influence. In fact, the simultaneous (i) absence of metallic particles (Sn or Ti) in the active material and (ii) detection of resonances shifted downfield suggest that a Knight shift or a close interaction of Li_3Sb with surrounding metallic particles are not the only cause of the observed downfield shifted resonances, as opposed to the conclusions detailed in reference 30.

To verify whether the resonance observed at −8.8 ppm in the current study corresponds to a non-stoichiometric phase of Li_3Sb, samples of Sb were cycled at C/2 and 4C and stopped at various stages towards the end of lithiation. To determine the phases formed, samples were stopped at potentials corresponding to points half way, two thirds of the way along and at the end of the plateau in the electrochemical lithiation profile, as shown in Figure S4 in the Supporting Information. Prior to NMR analysis, the samples were extracted, rinsed and dried. First of all, resonances are observed at 40 and −17 ppm in Figure S4, corresponding to Li_2Sb. The formation of Li_2Sb *during* the lithiation of Sb is in good agreement with previous XRD studies [12]. It is noted that exactly the same experimental conditions have been used here as in the recent TiSnSb study and the lithiation experiments discussed above. Hence, all of the data is comparable. The discrepancies observed are more than likely related to the depth of lithiation achieved during the lithiation process and the possible formation of surface vs. bulk species. There are other potential factors that could affect the local Li environments within the Li_3Sb structure. These are discussed in greater detail in the following sections (*vide infra*).

Consistently, in all cases, a resonance is observed at −7 ppm, believed to correspond to stoichiometric Li_3Sb (Figures S4(a)-(f)). A broad underlying resonance is observed around 0 ppm, believed to be SEI formation. In almost all cases, a low intensity resonance is also observed at 3.2 ppm, which was also visible in the study of Li_3Sb by Chang *et al.* [13]. Hence, two distinct shifts appear to be observed before completion of the lithiation process for Li_3Sb, at 3.2 and −7 ppm, respectively. These two resonances are not in a 1:1 ratio even at the end of the lithiation process. Moreover, their chemical shifts are quite different, suggesting their local environments are considerably different, which is not expected based on the two lithium sites described in the crystal structure. Therefore, the hypothesis of the detection of the two crystallographically distinct Li sites can be ruled out. Alternatively, the two distinct resonances could both correspond to Li_3Sb in different local and electronic environments. For example, the shift difference could be indicating a surface versus a bulk effect, *i.e.*, the resonance at negative shift seems to correspond to bulk Li_3Sb and the resonance at c.a. 4 ppm could be a surface species with a very different local environment. It is unknown whether one or both of these species is stoichiometric.

TiSnSb is known to undergo a conversion reaction that results in the formation of multiple nanocomposite structures. Hence, the Li_3Sb formed at the end of the lithiation of TiSnSb will likely be different to the 'bulk' Li_3Sb formed during mechanosynthesis. Similarly, the electrochemical lithiation of SnSb will produce a phase that is different to bulk Li_3Sb, *i.e.*, it will have a smaller particle size (*e.g.*, micro- or nano-sized domains) and, as a result, a larger surface area. NMR spectroscopy is sensitive to subtle changes in local coordination environments and surface/interface effects. Hence, any changes in particle size or the local structural or electronic Li environment will have a substantial effect on the corresponding ^7Li NMR parameters, particularly, the chemical shift. It is also noted that two additional elements are present in TiSnSb electrodes (Ti and Sn). This will undoubtedly affect the electronic properties and local environments of both the Li and Sb and the corresponding NMR spectra. Based on the data presented, and the works by Chang *et al*. [13] and Fernández-Madrigal *et al*. [30], we believe that the depth of lithiation (controlled by factors such as the rate of cycling and reaction mechanism) plays a key role in the Li-Sb phases formed at the end of lithiation and their relative chemical shifts. The presence of nearby metallic nanoparticles and the existence of non-stoichiometry are also believed to affect the electronic properties and local Li environments of the phases formed. Defects and non-stoichiometry are inherent to surfaces of particles. In the case of nanosized particles, obtained from electrochemical alloying or conversion reactions, such environments can become prominent, or at least in non-negligible/significant amounts.

Therefore, the significant downfield shifts observed for Li_3Sb-like phases can be due not only to interactions with surrounding metallic particles, as proposed in reference 30, but also due to modifications of local structural/electronic environments occurring for surface/non-stoichiometric environments. A defective surface could possibly alter the corresponding local electronic structure as does modification of the conduction bands in a metal (*i.e.*, Knight shift).

The Lithiation of Sn and SnSb

Samples of Sn and SnSb were lithiated to a cut-off potential of 10 mV at rates of C/2 and 4C. The corresponding electrochemical profiles are shown in Figures S5 and S6, respectively. After reaching the end of lithiation, each cell was immediately disassembled and the active materials were extracted. The ^{7}Li MAS NMR study is shown in the Supporting Information as it mostly confirms previous results [5, 6, 30-35]. Chemical shifts for all phases and Li local environments discussed in this article are detailed in Table 1.

The Lithiation of $TiSb_2$ and $NbSb_2$

To clarify the role played by the additional metallic species and their effect on the chemical shift of Li_3Sb, the alloys $TiSb_2$ and $NbSb_2$ were chosen for investigation because they contain Ti and Nb, elements that are not electrochemically active vs. Li. Such elements are typically used to limit or prevent volume changes of electrodes during electrochemical cycling. As a result, the only lithiated phase formed at the end of lithiation is Li_3Sb, as confirmed via XRD [36]. The ^7Li NMR spectra obtained for samples of $TiSb_2$ at the end of lithiation at C/2 and 4C (before and after 14 days) are shown in Figures 3(a) and S6(c), respectively. The spectra are similar in appearance, with a single broad resonance observed. A slight shouldering towards lower chemical shift is observed in each spectrum, suggesting the presence of multiple lithiated phases. However, since Ti (and Nb) is electrochemically inactive to Li, and there are no lithiated phases of Ti (or Nb) reported in the literature, it is unlikely additional Ti- (or Nb-) containing phases are present. Considerable differences in chemical shift are observed between the Li_3Sb formed here (10.8 and 11.9 ppm) and the Li_3Sb synthesized via ball milling and electrochemical methods (c.a −8 ppm). The ^7Li NMR spectra obtained for samples of $NbSb_2$ are shown in Figures 3(b) and S6(d). The spectra are very similar to those obtained for $TiSb_2$ and SnSb, *i.e.*, no distinct spectral features, just a single broad resonance centred at positive chemical shift. Again, Li_3Sb is the only phase expected to form at the end of lithiation. However, the observed chemical shift is quite different to that observed for Li_3Sb synthesized via mechanosynthesis or electrochemical methods. This is believed to be due to the following: (1) the local Li environment and electronic properties will be influenced by the formation of Ti (or Nb) nanoparticles at the end of lithiation and (2) a nanostructured phase of Li_3Sb is likely formed at the end of lithiation that has a smaller particle size relative to the 'bulk' phase. At the end of lithiation the alloy(s) formed are contained within a metallic matrix, which will result in interactions between the alloy(s) and the metallic species. This will, in turn, have a substantial effect on the local Li environments, *i.e.*, the electronic environment will be different. The chemical shift is controlled by factors such as the Knight shift, which is governed by the density of states at the Fermi level. 'Nanosizing' the alloys via the conversion reaction will have a substantial effect on the observed chemical shift because the particle size will have been changed.

Moreover, the chemical shifts are different in the spectrum obtained during the lithiation of $NbSb_2$ and $TiSb_2$. This indicates that changing the inactive metallic element from Ti to Nb has a substantial effect on the local Li environments, *i.e.*, changing the metal influences the interactions taking place between the metallic matrix and the phases formed. Hence, although the elements are electrochemically inactive, their presence is influencial.

For both $TiSb_2$ and $NbSb_2$, very little spectral evolution with time is observed for the samples cycled at C/2. However, samples cycled at 4C (Figures S6(c) and (d)) exhibit considerable evolution; the resonance shifts from 11.9 to 1.2 ppm for $TiSb_2$ and from 7.8 to −1 ppm for $NbSb_2$. This behaviour suggests that when cycled at rapid rates, the phase(s) formed at the end of lithiation are unstable and undergo some form of structural rearrangement to produce stable phases. In such cases, it is possible that the compositions of the phases formed are not changing substantially but internal inter-phase rearrangements are occurring. For example, there may be an interaction between the phases formed and the surrounding metallic matrix. The inactive element present in the initial alloy therefore influences the reaction that occurs during lithiation and, hence, the local Li environments of the phases formed. The inactive element also appears to have a direct effect on the reactivity and stability of the Li-based phases formed. A strong intimacy exists between the metallic Ti or Nb nanoparticles and Li_3Sb in the lithiated electrode. To investigate the conditions leading to such intimacy, electrodes made from mixtures of the same elements (Ti, Sn, Sb) were prepared and electrochemically tested.

<u>Mixtures – M1, M2 and M3</u>

The Lithiation of M1 and M2

When simple manual grinding is adopted, an intimate mixture of Sb and M elements is achieved, with micron distances between Sb and M independent grains. When high energy mechanosynthesis is employed, a MSb_x phase is formed, with angstrom distances between the atoms Sb and M in the MSb_x material. To evaluate the impact of the starting material upon the intimacy of mixing between Li_3Sb and M in the lithiated electrode, two mixtures of SnSb were prepared; one manually ground (M1) and one manually ground and ball milled for five minutes (M2). The XRD of M1 shows a mixture of Sn and Sb, whereas M2 shows a mixture of SnSb with residual Sn and Sb. Each sample was lithiated to a cut-off potential of 10 mV at rates of C/2 and 4C. After reaching the end of lithiation each cell was disassembled and the active materials were extracted, rinsed and dried. The corresponding ^{7}Li NMR spectra are shown in Figures 4 and S7, respectively. The spectrum for M1 is shown in Figure 4(a). It is broad and relatively featureless, suggesting a complex mix of Li-Sn and Li-Sb phases and a contribution from the SEI. There are some minor features at −8, 13.9, 42 and 78 ppm, assigned to Li_3Sb, Li_5Sn_2, LiSn and $Li_{22}Sn_5$, respectively [33]. This is in contrast to the spectrum for M2 in Figure 4(b), where distinct peaks are observed at −7.8 (Li_3Sb), 1.6 (Li_7Sn_2), 16.8 ($Li_{13}Sn_5$), 42 (LiSn), 32 (LiSn) and 78 ppm ($Li_{22}Sn_5$) [33]. A contribution from the SEI lies under the broad resonance centred around 0 ppm. The spectra acquired for mixtures M1 and M2 cycled at 4C are similar, with distinct features observed at −8 (Li_3Sb), 0 (SEI and Li_7Sn_2), 16 ($Li_{13}Sn_5$), 42 and 32 (LiSn) and 78 ppm ($Li_{22}Sn_5$) [33]. It is noted that the peaks are marginally sharper in the spectra for M2. This is to be expected as the sample will be more intimately mixed after even a short period of ball milling and therefore more homogeneous in its composition.

^{7}Li NMR spectra were acquired for all samples after a relaxation period and, in all cases, some evolution is observed with time. Differences in the peak intensities are observed, likely caused by small structural rearrangements of the highly reactive phases. However, no distinct differences in chemical shift are observed, suggesting the phases formed at the end of lithiation are relatively stable with time.

The Lithiation of M3

The mixture M3 (Ti+Sn+Sb), prepared via manual grinding, was lithiated to a cut-off potential of 10 mV at rates of C/2 and 4C. The corresponding ^{7}Li NMR spectra are shown in Figures 4(c) and S7(c), respectively. The spectrum acquired for M3 cycled at C/2 exhibits the same distinct features observed for M2 and is assigned the same, *i.e.*, −7.8 (Li_3Sb), 1.6 (SEI and Li_7Sn_2), 16.8 ($Li_{13}Sn_5$), 42 (LiSn), 32 (LiSn) and 78 ppm ($Li_{22}Sn_5$). The spectrum acquired for the sample cycled at 4C contains two broad resonances. Some distinct features are present at 42, 0, 1.6 and −8 ppm which are assigned to LiSn, SEI and Li_3Sb, respectively. A feature is also visible at −17 ppm. Based on the work by Chang *et al.*, this peak is assigned to Li_2Sb [13]. ^{7}Li NMR spectra were acquired for both samples after a relaxation period and, in both cases, little or no evolution is observed with time. Small changes in intensity are observed, however, there are no substantial changes in chemical shift, indicating the phases formed at the end of lithiation are stable with time.

In all of the mixtures discussed above, Li_3Sb is observed at negative chemical shift (c.a. −8 ppm). This is consistent with samples of isolated/bulk Li_3Sb synthesized via mechanosynthesis and electrochemical methods (*vide supra*). During the first lithiation, TiSnSb undergoes a conversion reaction. The lithiation of SnSb or Sn+Sb mixtures, however, is known to proceed via an alloying reaction [6, 31,37-39]. This difference in mechanism is believed to be a consequence of the initial mixing/synthesis. This influences the morphology and particle size of the active material. As previously demonstrated, during the first lithiation, TiSnSb undergoes a direct conversion reaction while Ti/Sn/Sb mixtures proceed via a stepwise alloying process, both leading to a mixture of lithium antimonide, lithium stannides and titanium [6]. More surprisingly, the delithiation occurs differently with a reformation of the "TiSnSb" phase in the first case and the formation of Sn and Sb in the second case [24]. As demonstrated by the NMR chemical shift evolution, at the end of lithiation of TiSnSb, Li_3Sb was observed at positive chemical shift (3.5 ppm), whereas for the Ti+Sn+Sb mixture (M3), Li_3Sb is observed at negative chemical shift, where, based on the current study, it is expected to appear. There are three, possibly combined, reasons for this: (1) the very intimate mixing between Ti/Sn/Sb in TiSnSb, which affects the local lithium environments and the observed chemical shifts, (2) the nature of the inactive element or, more specifically, the metallic nanoparticles formed at the end of lithiation have a substantial effect on the electronic properties of Li_3Sb or (3) the Li_3Sb formed at the end of lithiation via a conversion reaction is different to bulk Li_3Sb, *i.e.*, nano domains are formed meaning the particle size is much smaller and this influences the chemical shift or a surface-type species is formed [6]. This last point is, again, related to the very intimate mixing of the metals.

It is noted that this only appears to happen for Sb-based phases; Sn-based phases consistently appear at their reported chemical shifts. In the case of TiSnSb, this is likely providing information on the location of the Ti nanoparticles and their proximity to the Li-Sb and Li-Sn phases. The data presented suggests the metallic nanoparticles are closer to Li-Sb phases, as their shifts are severely affected by their presence. For example, nanoparticles could be 'clustering' close to or around Li_3Sb. Alternatively, the nanoparticles could be evenly distributed throughout the structure and Sb-based phases are simply more sensitive to their presence. It is, however, surprising that only the Li-Sb phases are affected by the presence of such highly reactive metallic nanoparticles.

The Lithiation of NbSnSb

To study the effects of the inactive element on chemical shift further, the ternary alloy NbSnSb has been investigated. NbSnSb is analogous to TiSnSb, the only difference is the inactive element; Nb and Ti, respectively [36]. Samples of NbSnSb were lithiated to a cut-off potential of 10 mV at rates of C/2 and 4C. After reaching the end of lithiation each cell was disassembled and the active materials were extracted, rinsed and dried. The corresponding ^{7}Li NMR spectra are shown in Figures 5 and S8(b), respectively. The spectrum obtained for the sample cycled at C/2 is very similar to that obtained for TiSnSb (Figure 5), *i.e.*, two broad, overlapped resonances. Nb, like Ti, is inactive to Li. Hence, if the conversion reaction is the same, the phases formed at the end of lithiation are expected to be exactly the same, *i.e.*, Li_3Sb, Li_7Sn_2, Li_7Sn_3 and a non-stoichiometric phase of Li_2Sb, $Li_{2-x}Sb$. As for TiSnSb, the phases Li_3Sb and Li_7Sn_2 have been confirmed via XRD and ^{119}Sn Mössbauer spectroscopy, respectively [40]. In the case of TiSnSb, two resonances were observed at 3.5 and 20 ppm in the ^{7}Li NMR spectrum (Figure 1). Here, resonances are observed at 1.4 and 17 ppm (Figure 5). These differences are substantial and appear to confirm previous discussions on the presence and influence of different inactive elements. The differences in chemical shift are clearly visible in Figure 5, where the spectra obtained for TiSnSb and NbSnSb at the end of lithiation are overlaid.

The spectrum obtained for NbSnSb cycled at 4C also displays two broad, overlapped resonances at 14.8 and 0.9 ppm (Figure S9). Again, the chemical shift of each resonance varies from that of lithiated TiSnSb. Moreover, it varies relative to the spectrum obtained for the sample cycled at C/2. Hence, it appears the cycling rate can also affect the chemical shifts of the phases formed. This is likely linked to the rate and depth of lithiation achieved, *i.e.*, faster cycling rates lead to lower depths of lithiation. A direct comparison of the spectra obtained for samples of TiSnSb and NbSnSb cycled at 4C is given in Figure S9(c). Considerable differences in chemical shift and peak intensity are observed. This highlights the differences observed when solely the inactive element M is changed. Spectra were acquired for all samples after a relaxation period and subtle changes in peak intensity were observed. For example, the peak at 14.8 ppm in the spectrum for NbSnSb cycled at 4C diminishes in intensity. This suggests that subtle structural rearrangements are taking place. However, no significant changes in chemical shift are observed, suggesting the phases formed are stable with time. Again, it is noted that no resonances are observed at negative chemical shift, where the resonance corresponding to Li_3Sb is expected to appear. This is believed to be a consequence of (1) the presence of additional elements, *e.g.*, Nb, Ti and Sn and (2) the precise conversion mechanism taking place.

The Lithiation of $Ti_{1-y}Nb_ySnSb$ (y = 0.25, 0.5 and 0.75)

Following the same logic, the same methodology was used to prepare samples in the series $Ti_{1-y}Nb_ySnSb$, *i.e.*, samples were prepared by ball milling then lithiated to a cut-off potential of 10 mV at rates of C/2 and 4C. The corresponding ^7Li NMR spectra (Figures 6, S10 and S11), are similar in appearance to the spectra obtained for TiSnSb (Figure 1) and NbSnSb (Figure 5), *i.e.*, two broad, overlapped resonances. Slight differences in chemical shift are observed depending on the precise composition of the sample, as shown in Figure 6. It is challenging to accurately assign all of the phases present due to significant spectral overlap. During the conversion reaction, both Ti and Nb nanoparticles are formed at the end of lithiation. Based on our earlier findings (*vide supra*), both will influence the chemical shifts of the phases formed. The spectra obtained for samples cycled at 4C exhibit greater differences in both chemical shift and peak intensity (Figure S11). The spectra obtained for $Ti_{0.25}Nb_{0.75}SnSb$ exhibit an additional resonance at 42 ppm, believed to be LiSn. Spectra were acquired for all samples after a relaxation period and the samples cycled at C/2 exhibit minor differences in peak intensity, with little or no change in the chemical shift (Figure S10). This is in contrast to the samples cycled at 4C where significant changes are observed with time (Figure S11). The sample $Ti_{0.5}Nb_{0.5}SnSb$ exhibits the greatest change, with almost the complete removal of the peak at ~20 ppm and an increase in the intensity of the resonance at ~3 ppm. This is similar to the behaviour previously reported for TiSnSb [24]. This suggests that the species formed at the end of lithiation are unstable and structural rearrangements occur in order for thermodynamically stable phases to be formed.

The spectra showin in Figure 6 could be providing insight into the location of the metallic nanoparticles. Comparing the spectra obtained for NbSnSb and $Ti_{0.5}Nb_{0.5}SnSb$, no significant differences in chemical shift are observed between the two and both spectra likely correspond to Li_xSb surrounded by a Nb metallic matrix. At higher Ti compositions, a progressive change in the chemical shift is observed. This behaviour suggests the Li_xSb phases prefer to be surrounded by Nb and it is only when there is no longer enough Nb that some Ti is nearby these Li_xSb phases. This then changes their local electronic environment and modifies their NMR shifts. This is an important finding as this could be key to the success of the conversion reaction occurring within all these samples. Conversion materials such as TiSnSb have high energy densities which are believed to be a consequence of the conversion reaction occurring. The data presented suggests the inactive element present could greatly influence or affect the success of the conversion process. For example, even though the ternary alloy containing Ti exhibits a higher capacity relative to the alloy containing Nb, *i.e.*, 500 mA·h/g (TiSnSb) vs. 450 mA·h/g (NbSnSb), NbSnSb is found to exhibit better cycling performance longer term, in particular concerning coulombic efficiency [7]. The findings suggest this is due to the reactivity of the metallic nanoparticles formed during the conversion reaction and/or the preference of Li_3Sb to be surrounded by Nb instead of Ti where possible. Hence, the inactive element used to reduce the volume expansion of electrodes could actually be one of the most important and influencial elements in the alloy.

Coulometric Titration of TiSnSb, $Ti_{0.5}Nb_{0.5}SnSb$, and NbSnSb

To study the diffusion process and gain insights into the thermodynamics and kinetics of these alloying electrodes, coulometric titration experiments were undertaken. A current pulse equivalent to a rate of C/10 was applied for thirty minutes (*i.e.*, 1/20th theoretical capacity based on $Li_{6.5}MSnSb$), followed by a 12 h rest where the potential was allowed to relax from the initial closed-circuit voltage (V_{cc}) toward the thermodynamic open-circuit voltage (V_{oc}). Using the method of Weppner and Huggins discussed previously for Li_3Sb, chemical diffusion coefficients for lithium ($\tilde{D}_{Li}$) were calculated. The major source of error in this calculation is the diffusion distance (L), which varies in its interpretation from particle (nm–µm) to film (*ca.* 100 µm) thickness. In reality, there are multiple diffusion timescales in a heterogeneous electrode film with a distribution of particle sizes. Fortunately, this error is relative and so we consider the value of $\tilde{D}_{Li}$ as a function of potential and between the various MSnSb compositions rather than the absolute magnitude. In these electrode materials, there is an order-of-magnitude decrease in $\tilde{D}_{Li}$ during litihiation (Figure 7). The minima shift to lower potentials as Ti is substituted for Nb in the structure but the overall shape and magnitude of the diffusion profile is otherwise compositionally independent. Interestingly, at the end of the lithiation process (V_{oc} < 0.2 V), the diffusion coefficient increases to approximately the same value as in the dilute limit Li_xMSnSb at the onset of lithiation. The redox-innocent metal appears to affect the potential of alloy phase formation and thus the potential where diffusion limitations are most significant, confirming the strong influence of the so-called inactive element on the electrochemical behavior and performance. This result is particularly relevant for commercial cells because it implies differential rate performance as a function of voltage.

Further Discussion

The presence of Li_3Sb at two distinct chemical ^7Li NMR shifts is particularly interesting. Based on the current findings, both chemical environments are believed to be stoichiometric phases. However, their local environments or, more specifically, their local electronic structures are believed to be quite different. The resonance observed at negative chemical shift (~ −8 ppm) is believed to correspond to the "bulk" Li_3Sb obtained in isolation via ball milling or electrochemical synthetic methods (*e.g.* from lithiation of Sb electrodes). The resonance observed at positive chemical shift (~ 4 ppm) is believed to be either a lithiated surface species or a bulk form of Li_3Sb that exhibits a substantially different or altered electronic environment owing to strong interactions with the surrounding metallic matrix. The defects and dangling bonds inherent to "surface species" could alter the local electronic Li environment significantly and such an environment could become prominent in the Li_3Sb nano-sized particles formed. The latter is believed to be a direct consequence of both the intimate mixing of the metallic species during synthesis (*i.e.*, during the ball milling phase) and the conversion reaction occurring. Theoretical calculations are necessary to fully understand the two effects and determine how they affect the observed ^7Li NMR shift but such a study is out of the scope of the current article. We know that changing the electrochemically inactive species will alter the electronic environment and, hence, the observed chemical shift, as demonstrated by the NbSnSb study (*vide supra*).

Comparing chemically identical but structurally different electrodes (*i.e.*, ternary alloys vs. mixtures) highlights the structural importance of the intimacy of mixing of the elements (Sb, Sn, M) in the initial electrodes. Thus, the ^{7}Li NMR data obtained suggests that the more or less intimate mixture between these elements has a substantial influence on (1) the reaction during lithiation (*i.e.*, conversion vs. alloying), (2) the phases formed at the end of lithiation and (3) the stability of the phases formed.

Concerning the latter point, it is interesting to compare the behaviour of the different materials investigated here in terms of their stability during a relaxation period after the end of lithiation. In the case of TiSnSb, the instability of some of the reduced species were first observed in a previous study by our groups [24]. This study suggested two distinct processes occurring during the evolution period of TiSnSb, after lithiation. The first process has been assigned to a thermodynamic equilibration of the system, where the highly reactive/metastable Li−Sb and Li−Sn phases formed at the end of lithiation (induced by optimal nanosized interfaces) undergo structural rearrangements and/or phase transitions to produce more intrinsically stable intermetallics. This first process does not lead to loss of lithium. The second process occurring, and favoured in the presence of electrolyte, seems to be a spontaneous loss of Li and the species created at the end of discharge evolve towards delithiated phases. This second process corresponds to a self-discharge process. The respective contribution of the presence of these optimal nanosized interfaces and the presence the so-called metallic “inactive” element to the relaxation behavior, although established, could not be discriminated. Since samples in the current study were rinsed prior to *ex situ* NMR experiments (to remove the influence of electrolyte), we expect to observe only the first process corresponding to subtle structural rearrangement.

Looking at the evolution of the ^{7}Li NMR spectra after lithiation for Sb, Sn and SnSb electrodes (Figures 2, S5, S6(a) S6(b)), the absence of evolution after a relaxation period indicates that the phases formed are stable with time. It shows clearly that the intimate mixing of elements and nanosized interfaces, notably in the case of the SnSb alloy is not sufficient to provoke rearrangement between reduced phases, irrespective of the cycling rate (C/2 or 4C). Now, considering the case of the mixture prepared by manual grinding: After the relaxation period, only slight differences in the peak intensities are observed, both for C/2 and 4C lithiation (Figure 4 and S7). Although these changes are likely caused by small structural rearrangements of the highly reactive phases, no distinct differences in chemical shift are observed and Li environments detected in small amounts are still present after evolution. This suggests that the presence of Ti and Nb have an influence, probably because interfaces between the different reduced phases exist but the phases formed at the end of lithiation are separated by microsized rather than nanosized interfaces and thus not optimized. This is confirmed by the presence of the Li_3Sb resonance at negative chemical shift, corresponding to the “isolated” Li_3Sb, not in contact with Ti nanoparticles.

Combining an “inactive” metallic element such as Ti or Nb, as well as an intimate mixing, appears to be necessary to achieve this instability and rearrangements of the lithiated phases. In binary or ternary alloys (containing the “inactive” element) prepared via high energy ball milling, all of the elements are intimately and homogeneously mixed with one another, producing a phase (from a crystallographic point of view), where there is a maximum proximity of atoms that are perfectly ordered. As a result, the phases formed at the end of lithiation are in very close contact with one another and the metallic nanoparticles via nanosized interfaces. In the case of $TiSb_2$, $NbSb_2$ and the $Ti_{1-y}Nb_ySnSb$ solid solution: significant evolutions are observed after a lithiation at 4C. For example, the sample $Ti_{0.5}Nb_{0.5}SnSb$ exhibits the greatest change in its ^7Li MAS NMR spectrum, with almost the complete removal of the peak at ~20 ppm and an increase in the intensity of the resonance at ~3 ppm. Significant internal inter-phase rearrangements, due to an enhanced interaction between the phases formed and the surrounding metallic matrix, are also observed in the case of $TiSb_2$ and $NbSb_2$. Overall, the lithiated phases formed from $TiSb_2$ and $NbSb_2$ at 4C seem somehow less stable than in the case of the alloys containing Sn. This suggests a stabilizing effect of the presence of Sn or rather Li_xSn phases, which are not metallic. The greater instability at 4C, when observed, could be due to a lower depth of lithiation leading to a different balance/amount of lithiated phases and/or inhomogeneities at the electrode scale. Overall, a low rate of cycling (such as C/2) yield higher stability for the lithiated phases. Finally, lithiated NbSnSb shows only subtle rearrangement/evolution after a relaxation period and seems to be more stable than its TiSnSb counterpart. More changes are observed in the case of TiSnSb (in line with the previous reported study [24]). The evolution of chemical shifts in the $Ti_{1-y}Nb_ySnSb$ solid solution, indicated that the lithiated phases were preferentially, when possible, surrounded by Nb metallic particles instead of Ti nanoparticles. This supports a higher stability of the different phases when surrounded by Nb particles that could explain the less evolution observed in the case of NbSnSb with respect to TiSnSb after their respective lithiation.

The data presented suggests the metallic nanoparticles strongly affect the electronic environment of lithium in the lithiated phases formed during the conversion process and, as a result, could have a substantial effect on the materials performance and its ability to act as an electrode material. The modifications of local structural/electronic environments occurring for surface/non-stoichiometric environments, as observed by significant downfield NMR shifts for Li_3Sb-like phases, can be reasonably expected to influence the electrochemical performance and lithiation/delithiation mechanism. Moreover, in the case of nano-sized particles, obtained from electrochemical alloying or conversion reactions, such environments can become prominent. Marino *et al.* and Coquil *et al.* [6,7] investigated the electrochemical performance of TiSnSb and NbSnSb, respectively. The two materials displayed excellent performance. The presence of Ti or Nb as an "inactive" element therefore leads to promising performance and it seems difficult to discriminate them at low cycling rate. This suggests that the instability of the reduced species is reversible and does not have a negative impact on the electrochemical cycling. At 8C, the capacity retention of TiSnSb is lower and the specific capacity falls from 400 to 270 mA/g in 150 cycles [6]. NbSnSb seems to be able to sustain 400 mAh/g for a few cycles, as shown by a rate capability test [7] and is shown to exhibit better cycling performance longer term, in particular the coulombic efficiency [7]. The role of the inactive element M or the instability of the lithiated phases may become important only in "extreme" conditions (*e.g.*, long cycling, fast cycling rate) and should be investigated further to establish the precise effect on the electrochemical performance. This could provide valuable information and insight into the future design of conversion materials for use in Li-ion batteries. Hence, further investigation is required to determine the M, "inactive element", that will provide the greatest properties and *in fine* the best performance in batteries.

Conclusions

To understand the phases formed at the end of lithiation, samples of TiSnSb were studied via XAS and ^{7}Li MAS spectroscopies. XAS clearly confirms the formation of Ti nanoparticles in close contact with Sn/Sb species during the lithiation of TiSnSb. Upon delithiation, these very reactive nanoparticles are transformed back and re-introduced into an amorphous phase structurally close to the initial one, with restored Ti-Sn and Ti-Sb bonds, confirming the expected conversion reaction mechanism already observed in previous work.

Several model metallic systems were investigated using ^{7}Li MAS NMR spectroscopy. The results indicate that the phases formed at the end of lithiation and their respective NMR shifts are influenced by a number of factors, including (1) the intimacy of mixing during the initial synthesis (*i.e.*, whether the species is a phase or simple mixture of elements), (2) the elements present in the alloy or mixture, particularly the electrochemically inactive element M and (3) the precise reaction occuring, *i.e.*, alloying vs. a conversion reaction.

The lithiation of Sb was initially investigated via both mechanosynthesis and electrochemical methods and, in both cases, the "isolated" Li_3Sb phase was consistently observed at negative chemical shift (c.a. −8 ppm), in agreement with previous studies.

When Li_3Sb is formed in the presence of metallic nanoparticles, in strong interaction, *e.g.*, in the case of ternary or binary alloys such as TiSnSb, NbSnSb, $TiSb_2$, $NbSb_2$ or SnSb, the chemical shift is altered substantially relative to that observed during the lithiation of Sb. This was confirmed by studies of both mixtures and alloys. The chemical shift was found to vary depending on the intimacy of the mixing during synthesis and the nature of the other elements present, particularly the electrochemically inactive species. The effect of the electrochemically inactive element M proved to be particularly interesting. When both mixtures and alloys prepared with the same elements were compared the observed ^7Li chemical shifts were notably different. The results suggest that some elements may be better than others for enabling alloying or conversion reactions to occur. In ternary alloys such as TiSnSb and NbSnSb there appears to be very complex interactions between the metallic matrix formed and the Li-Sn and Li-Sb phases present, as shown by the Ti K-edge XAS results.

From the study of the lithiation of a Sb electrode, it appears that the presence of nearby metallic nanoparticles is not the only feature to affect the electronic properties and local Li environments in Li_3Sb, as was previously proposed. Defects and non-stoichiometry, which are inherent to surfaces of particles, also lead to similar observed NMR shifts for Li_3Sb environments. It appears that a significant downfield shift observed for Li_3Sb-like phases can be due to modifications of local structural/electronic environments occurring for surface/non-stoichiometric environments. In the case of nano-sized particles, obtained from electrochemical alloying or conversion reactions, such environments can become prominent or at least in non-negligible/significant amounts.

Lithiation of the series $Ti_{1-y}Nb_ySnSb$ proved to be highly informative. At high Ti compositions a distinctive change in the ^7Li chemical shift is observed, suggesting Li_xSb phases prefer to be surrounded by Nb nanoparticles rather than Ti. It is likely this is influencing the conversion reaction occurring and the reactivity of the phases formed.

Finally, changes occurring during a relaxation period for the different compounds (mixtures, binary and ternary alloys) were compared. The influence of the presence of the metallic "inactive" element, the influence of the intimate mixing that can only be obtained in the case of binary and ternary alloys, the nature of the "inactive" metallic element as well as the cycling conditions (C/2 vs. 4C) were all discussed. The intimate mixing of elements and nanosized interfaces or the presence of the inactive elements alone are not sufficient to provoke structural rearrangements and/or phase transitions towards more intrinsically stable intermetallics whatever the cycling rate (C/2 or 4C). It is this combination of highly reactive species with close contacts (nanosized interfaces) including with Ti or Nb nanoaprticles that is responsible for the instability observed. The higher stability of the different phases when surrounded by Nb particles, instead of Ti, could explain the better cycling performance of NbSnSb, particularly the coulombic efficiency during extended cycling.

To fully understand the conversion mechanism, we need to understand the contribution from the metallic nanoparticles and the electronic interactions between them and lithiated alloys. Moreover, to improve the performance of conversion materials we need to study and understand the effects of *different* inactive elements. This will be essential if this class of materials is to be commercialized and used as negative electrodes in the future.

Author Contributions

Karen E. Johnston (K.E.J) : experimental investigation, electrochemical cycling, MAS NMR experiments, data analysis, scientific discussion, manuscript writing, editing and revision. Ali Darwiche (A.D.): Synthesis, Electrode formulation and preparation, X-ray diffraction. Lorenzo Stievano (L.S.): X-ray Absorption Spectroscopy experiments and analysis, scientific discussion, manuscript editing. Kent J. Griffith (K.J.G.): coulometric titration experiments. Nicolas Dupré (N.D): project conception, scientific discussion, manuscript editing. Laure Monconduit (L.M.): project conception, scientific discussion, manuscript editing. Clare P. Grey (C.P.G.): project conception, scientific discussion, manuscript editing

Acknowledgements

This research was performed in the framework of the ALISTORE European Research Institute and their Mössbauer and NMR platforms. The authors thank ALISTORE-ERI for its financial support through the postdoc grant of KEJ, the ANR for financial support in the program ICARES (no. ANR-11BS09-009-01) and in the project Labex STORE-EX (Grant ANR-10-LABX-76-01). Synchrotron ELETTRA Trieste is thanked for beamtime at beamline XAFS. Andrea Cognigni, Guiliana Aquilanti and Luca Olivi are gratefully acknowledged for expert advice on beamline operation. LM thanks all partners of the ICARES project for fruitful scientific discussions.

Supporting Information Available: Additional electrochemical, XANES, EXAFS and ^{7}Li NMR data.

References

[1] P.G. Bruce, B. Scrosati, J.M. Tarascon, Nanomaterials for rechargeable lithium batteries, Angew. Chem., Int. Ed. 47 (2008) 2930-2946.

[2] M.R. Palacin, Recent advances in rechargeable battery materials: a chemist's perspective, Chem. Soc. Rev. 38 (2009) 2565-2575.

[3] J. Wang, I.D. Raistrick, R.A. Huggins, Behavior of Some Binary Lithium Alloys as Negative Electrodes in Organic Solvent-Based Electrolytes, J. Electrochem. Soc. 133 (1986) 457-460.

[4] C. Villevieille, C.M. Ionica-Bousquet, B. Ducourant, J.C. Jumas, L. Monconduit, $NiSb_2$ as negative electrode for Li-ion batteries: An original conversion reaction, J. Power Sources 172 (2007) 388-394.

[5] M.T. Sougrati, J. Fullenwarth, A. Debenedetti, B. Fraisse, J. C. Jumas, L. Monconduit, TiSnSb a new efficient negative electrode for Li-ion batteries: mechanism investigations by *operando*-XRD and Mössbauer techniques, J. Mater. Chem. 21 (2011) 10069-10076.

[6] C. Marino, M.T. Sougrati, B. Gerke, R. Pöttgen, H. Huo, M. Ménétrier, C.P. Grey, L. Monconduit, Role of Structure and Interfaces in the Performance of TiSnSb as an Electrode for Li-Ion Batteries, Chem. Mater. 24 (2012) 4735-4743.

[7] G. Coquil, M.T. Sougrati, S. Biscaglia, D. Ayme-Perrot, P.F. Girard, L. Monconduit, On the high cycling stability of NbSnSb in Li-ion batteries at high Temperature, Electrochim. Acta 281 (2018) 619-623.

[8] C.M. Park, H.J. Sohn, Electrochemical characterisation of $TiSb_2$ and Sb/TiC/C nanocomposites as anodes for rechargeable Li-ion batteries, J. Electrochem. Soc. 157 (2010) A46-A49.

[9] W. Weppner, R.A. Huggins, Thermodynamic properties of intermetallic systems lithium-antimony and lithium-bismuth, J. Electrochem. Soc. 125 (1978) 7-14.

[10] J. Sangster, A.D. Pelton, The K-Sb (Potassium-Antimony) system, J. Phase Equilib. 14 (1993) 510-514.

[11] K.C. Hewitt, L.Y. Beaulieu, J.R. Dahn, Electrochemistry of InSb as a Li Insertion Host: Problems and Prospects, J. Electrochem. Soc. 148 (2001) A402-A410.

[12] C.J. Wen, R.A. Huggins, Thermodynamic study of the lithium-tin system, J. Electrochem. Soc. **128 (**1981) 1181-1187.

[13] D. Chang, H. Huo, K.E. Johnston, C. Marino, L. Monconduit, C.P. Grey, A. van der Ven, Elucidating the origins of phase transformation hysteresis during electrochemical cycling of Li–Sb electrodes, J. Mater. Chem. A 3 (2015) 18928-18943.

[14] D.A. Hansen, L.J. Chang, Crystal structure of Li_2Sn_5, Acta Crystallogr. B 25 (1969) 2392-2395.

[15] W. Müller, H. Schäfer, The crystal structure of LiSn, Z. Naturforsch. 28b (1973) 246-248.

[16] W. Müller, Preparation and crystal structure of Li_7Sn_3, Z. Naturforsch. 29b (1974) 304-307.

[17] U. Frank, W. Müller, H. Schäfer, The crystal structure of Li_5Sn_2, Z. Naturforsch. 30b (1975) 1-5.

[18] U. Frank, W. Müller, Preparation and crystal structure of $Li_{13}Sn_5$ and the structural relations between the phases of the systems Li-Sn and Li-Pb, Z. Naturforsch. 30b (1975) 316-322.

[19] U. Frank, W. Müller, H. Schäfer, The crystal structure of Li_7Sn_2, Z. Naturforsch. 30b (1975) 609-615.

[20] E.I. Gladyshevskii, G.I. Oleksiv, P.I. Kripyakevich, New specimens of the structural type $Li_{22}Pb_5$, Kristallografiya 9 (1964) 338-341.

[21] J. Chouvin, J. Olivier-Fourcade, J.C. Jumas, B. Simon, O. Godiveau, ^{119}Sn Mössbauer study of Li_xSn alloys prepared electrochemically, Chem. Phys. Lett. 308 (1999) 413-420.

[22] R.A. Dunlap, D.A. Small, D.D. MacNeil, M.N. Obrovac, J.R. Dahn, A Mössbauer effect investigation of the Li–Sn system, J. Alloys Compd. 289 (1999) 135-142.

[23] F. Robert, P.E. Lippens, J. Olivier-Fourcade, J.C. Jumas, F. Gillot, M. Morcrette, J.M. Tarascon, Mössbauer spectra as a "fingerprint" in tin-lithium

compounds: Applications to Li-ion batteries, J. Solid State Chem. 180 (2007) 339-348.

[24] K.E. Johnston, M.T. Sougrati, L. Stievano, A. Darwiche, N. Dupré, C.P. Grey, L. Monconduit, The effects of relaxation on conversion negative electrode materials for Li-ion batteries : a study of TiSnSb using ^{119}Sn Mössbauer and ^{7}Li MAS NMR spectroscopies, Chem. Mater. 28 (2016) 4032-4041.

[25] M. Fehse, A. Darwiche, M.T. Sougrati, E.M. Kelder, A.V. Chadwick, M. Alfredsson, L. Monconduit, L. Stievano, In-Depth Analysis of the Conversion Mechanism of TiSnSb vs Li by Operando Triple-Edge X-ray Absorption Spectroscopy: a Chemometric Approach, Chem. Mater. 29 (2017) 10446−10454.

[26] J.J. Rehr, J. Mustre de Leon, S.I. Zabinsky, R.C. Albers, Theoretical X-ray absorption fine structure standards, J. Am. Chem. Soc. 113 (1991) 5135-5140.

[27] E. Dashjav, H. Kleinke, Sn/Sb atom ordering in the ternary stannide-antimonide TiSnSb, J. Solid State Chem. 176 (2003) 329-337.

[28] J.B. Leriche, S. Hamelet, J. Shu, M. Morcrette, C. Masquelier; G. Ouvrard, M. Zerrouki, P. Soudan, S. Belin, E. Elkaim, F. Baudelet, An electrochemical cell for operando study of kithium batteries using synchrotron radiation, J. Electrochem. Soc. 157 (2010) A606-A610.

[29] D. Massiot, F. Fayon, M. Capron, I. King, S. Le Calvé, B. Alonso, J.O. Durand, B. Bujoli, Z. Gan, G. Hoatson, Modelling one and two-dimensional solid-state NMR spectra, Magn. Reson. Chem. 40 (2002) 70-76.

[30] F.J. Fernández-Madrigal, P. Lavela, C.P. Vicente, J.L. Tirado, X-ray diffraction, ^{7}Li MAS NMR spectroscopy and ^{119}Mössbauer spectroscopy study of SnSb-based electrode materials, Chem. Mater. 14 (2002) 2962-2968.

[31] P. Antitomaso, B. Fraisse, L. Stievano, S. Biscaglia, D. Aymé-Perrot, P. Girard, M. T. Sougrati, L. Monconduit, SnSb electrode for Li-ion batteries: electrochemical mechanism and capacity fading origins elucidated by Operando techniques, J. Mat. Chem. A 5 (2017) 6546-6555.

[32] C. Marino, A. Darwiche, N. Dupre, H.A. Wilhelm, B. Lestriez, H. Martinez, R. Dedryvère, W. Zhang, F. Gamouss, D. Lemordant L. Monconduit, Study of the Electrode/Electrolyte Interface on Cycling of a Conversion Type Electrode Material in Li Batteries, J. Phys. Chem. C 117 (2013) 19302-19313

[33] E. Bekaert, F. Robert, P.E. Lippens, M. Ménétrier, ^{7}Li NMR knight shifts in Li-Sn compounds: MAS NMR measurements and correlation with DFT calculations, J. Phys. Chem. C 114 (2010) 6749-6754.

[34] J.O. Besenhard, M. Wachtler, M. Winter, R. Andreaus, I. Rom, W. Sitte, Kinetics of Li insertion into polycrystalline and nanocrystalline 'SnSb' alloys investigated by transient and steady state techniques, J. Power Sources 81-82 (1999) 268-272.

[35] M. Winter, J.O. Besenhard, Electrochemical lithiation of tin and tin-based intermetallics and composites, Electrochim. Acta 45 (1999) 31-50.

[36] C. Marino, M.T. Sougrati, A. Darwiche, J. Fullenwarth, B. Fraisse, J.C. Jumas, L. Monconduit, Study of the series $Ti_{1-y}Nb_ySnSb$ with $0 \leq y \leq 1$ as anode materials for Li-ion batteries, J. Power Sources 244 (2013) 736-741.

[37] H.Z. Dokuzoguz, L.H. Bowen, H.H. Stadelmaier, Isomer shifts of ^{121}Sb in III–V semiconductors, Solid State Commun. 8 (1970*)* 259-261.

[38] R.A. Pruitt, S.W. Marshall, C.M. O'Donnell, Mössbauer Spectroscopy in Group-III Antimonides, Phys. Rev. B 2 (1970) 2383-2390.

[39] L. Aldon, A. Garcia, J. Olivier-Fourcade, J.C. Jumas, F.J. Fernandez-Madrigal, P. Lavela, C.P. Vicente, J.L. Tirado, Lithium insertion mechanism in Sb-based electrode materials from Sb-121 Mossbauer spectrometry, J. Power Sources 119 (2003) 585-590.

[40] C. Marino, B. Fraisse, M. Womes, C. Villevieille, L. Monconduit, L. Stievano, At the Heart of a Conversion Reaction : An Operando X-ray Absorption Spectroscopy Investigation of NiSb2, a Negative Electrode Material for Li-ion Batteries, J. Phys. Chem. C 118 (**2014**) 27772-27780.

Figures:

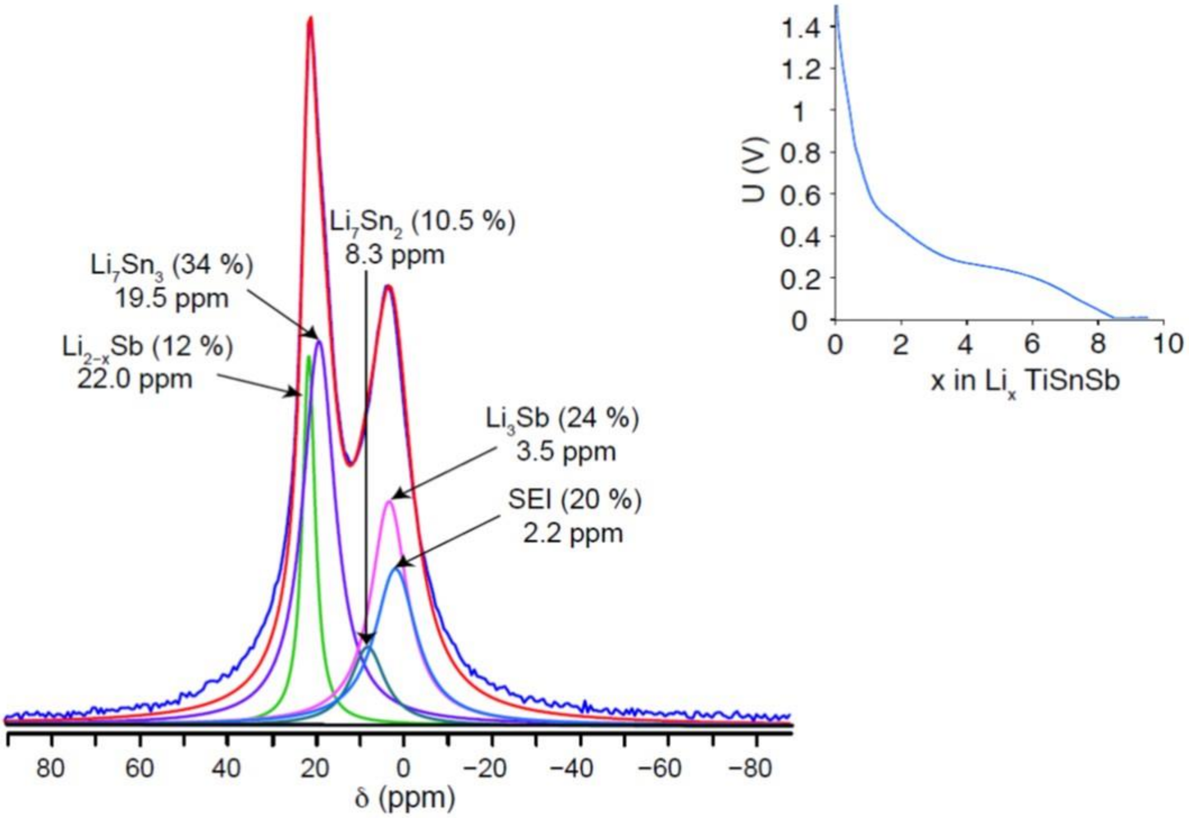

Figure 1: Deconvolution of the ^{7}Li (4.7 T) MAS NMR spectrum obtained at the end of lithiation of TiSnSb. The sample was cycled at C/2 and the MAS rate was 25 kHz. Shown as an inset is the corresponding electrochemical profile.

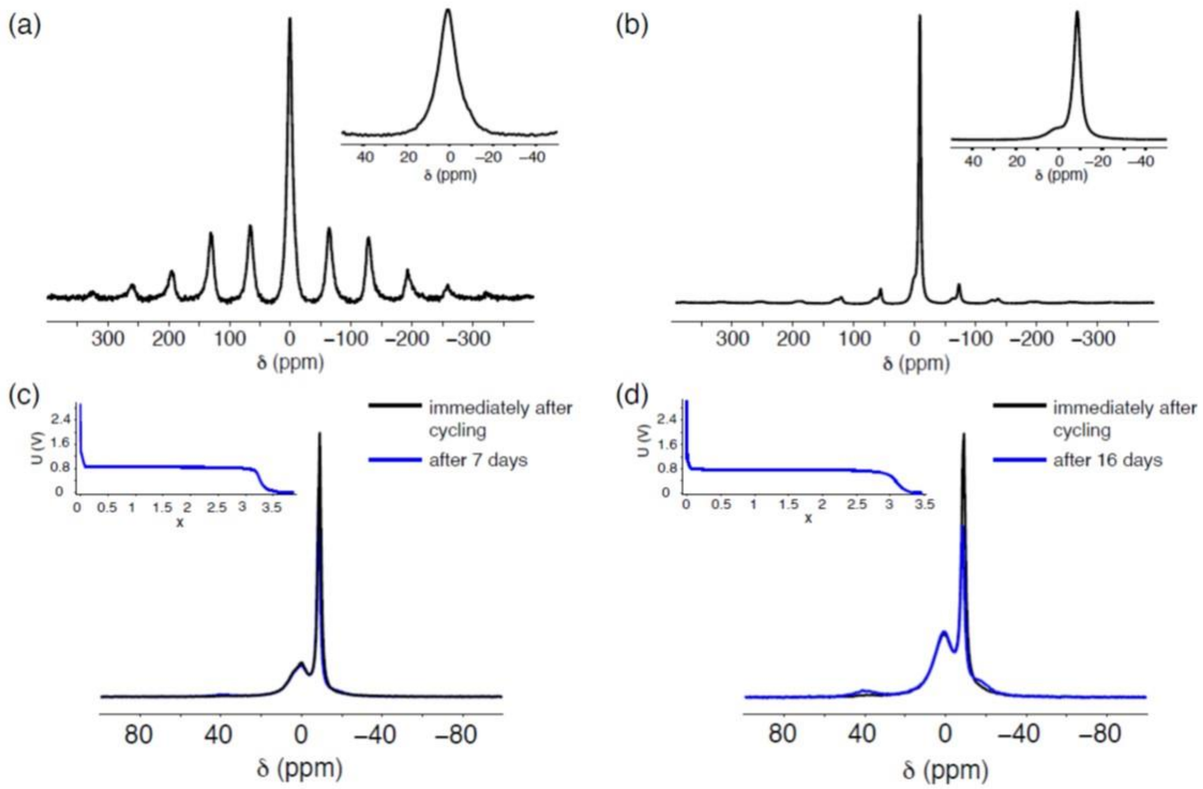

Figure 2: ^{7}Li (4.7 T) MAS NMR spectra obtained for (a) Li_2Sb and (b) Li_3Sb prepared via solid state methods and pure Sb electrochemically cycles at rates of (c) C/2 and (d) 4C. In (c) and (d) the spectra obtained immediately after reaching the end of lithiation are shown in black and the spectra obtained after a relaxation period are shown in blue. The MAS rate was 25 kHz. Also shown in (c) and (d) are the corresponding potential profiles for Sb.

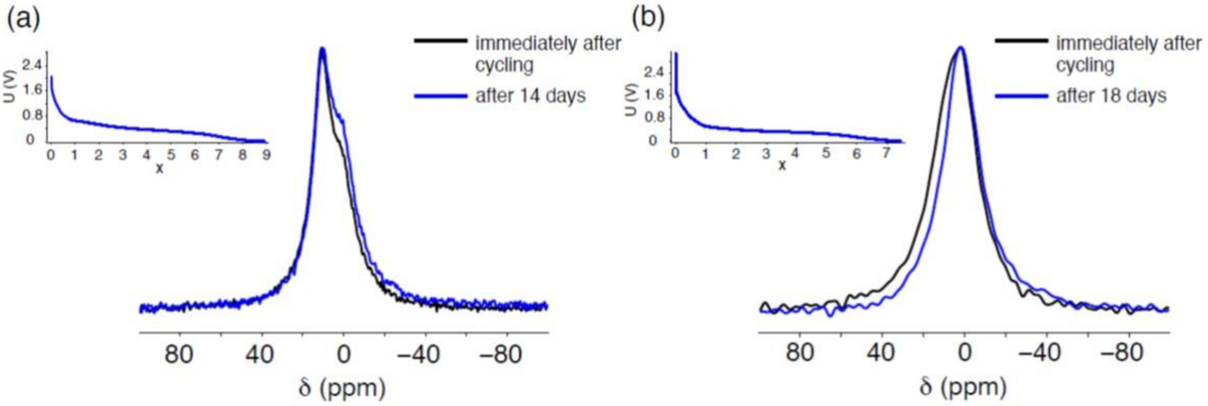

Figure 3: ^{7}Li (4.7 T) MAS NMR spectra obtained after electrochemical cycling of (a) $TiSb_2$ and (b) $NbSb_2$. All samples were cycled at a rate of C/2. In each case, spectra obtained immediately after reaching the end of lithiation are shown in black and spectra obtained after an additional relaxation period are in blue. The MAS rate was 25 kHz. Also shown as insets are the potential profiles obtained for each.

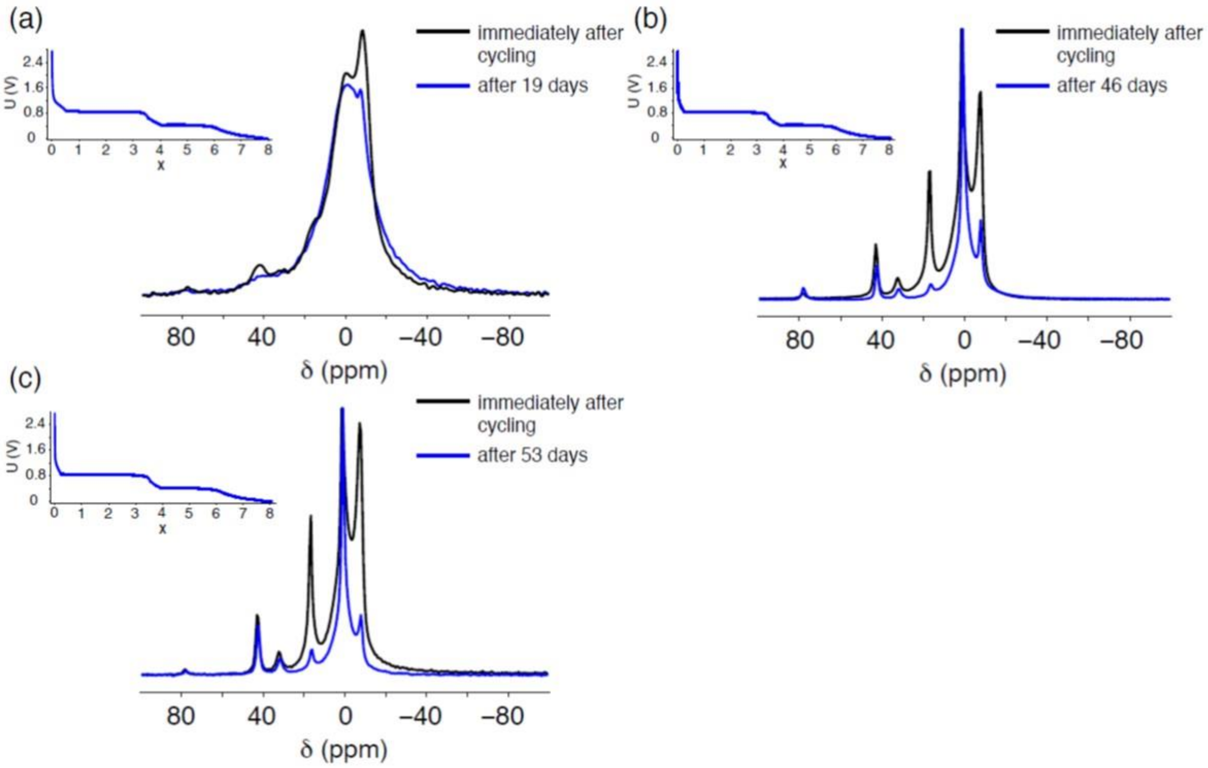

Figure 4: ^{7}Li (4.7 T) MAS NMR spectra obtained after electrochemical cycling of composites (a) M1, (b) M2 and (c) M3. All samples were cycled at C/2. In each case, spectra obtained immediately after reaching the end of lithiation are shown in black and spectra obtained after an additional relaxation period are in blue. The MAS rate was 25 kHz. Also shown as insets are the potential profiles obtained for each.

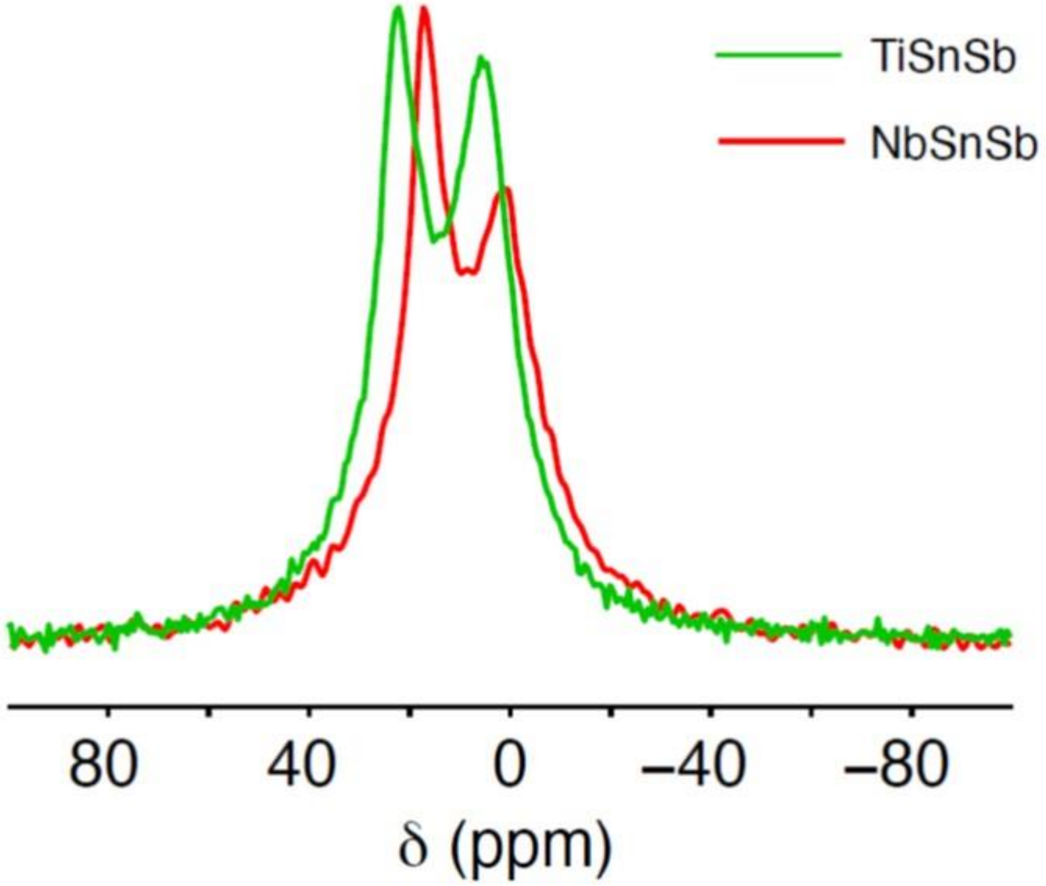

Figure 5: ^{7}Li (4.7 T) MAS NMR spectra obtained immediately after electrochemical cycling to the end of lithiation for TiSnSb and NbSnSb. Both samples were cycled at a rate of C/2. The MAS rate was 25 kHz.

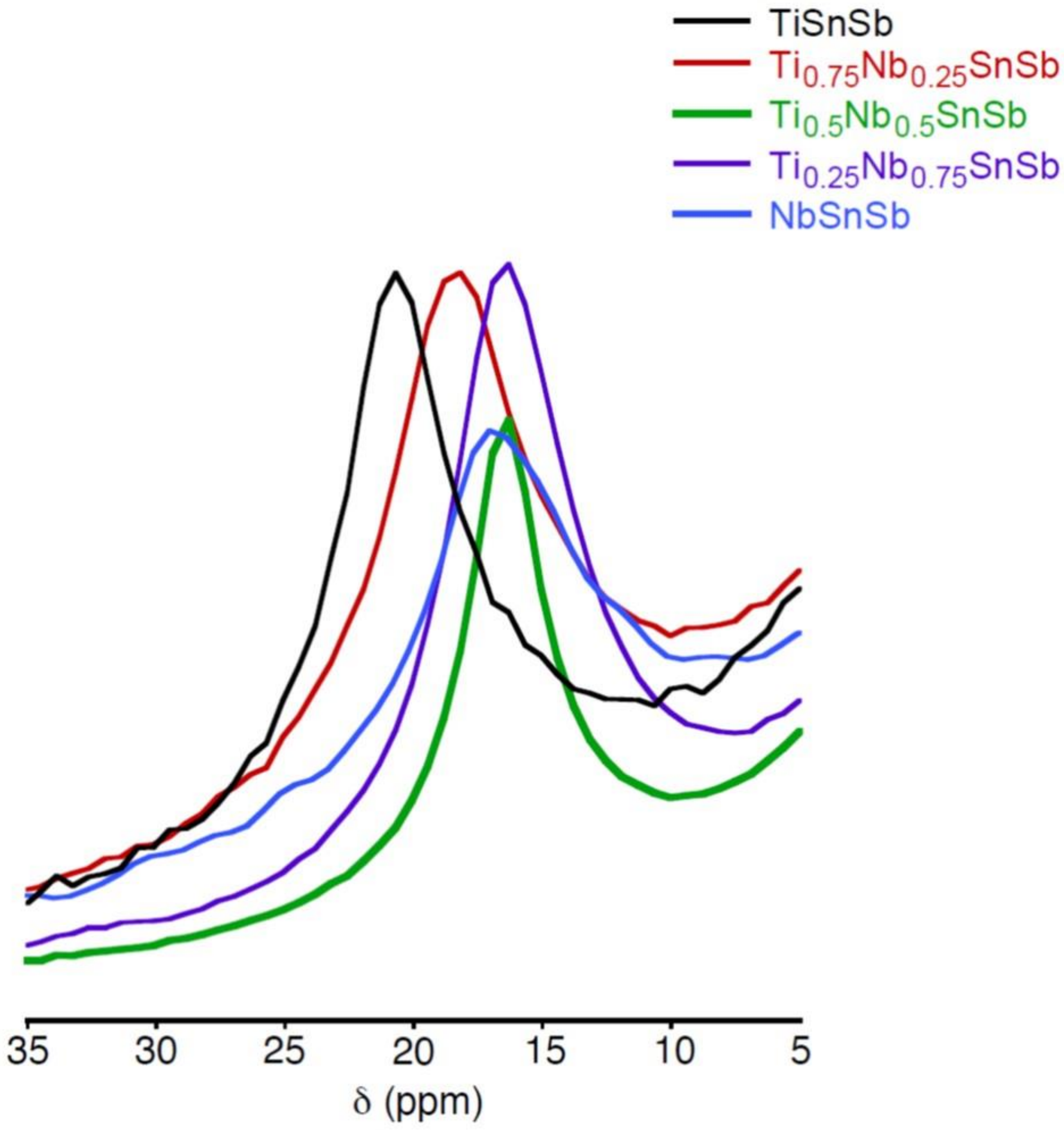

Figure 6: Expansion of the ^{7}Li (4.7 T) MAS NMR spectra obtained after electrochemical cycling to the end of lithiation for TiSnSb (black), $Ti_{0.75}Nb_{0.25}SnSb$ (red), $Ti_{0.5}Nb_{0.5}SnSb$ (green), $Ti_{0.25}Nb_{0.75}SnSb$ (purple) and NbSnSb (blue). Complete spectra are given in Figure S9 in the Supporting Information.

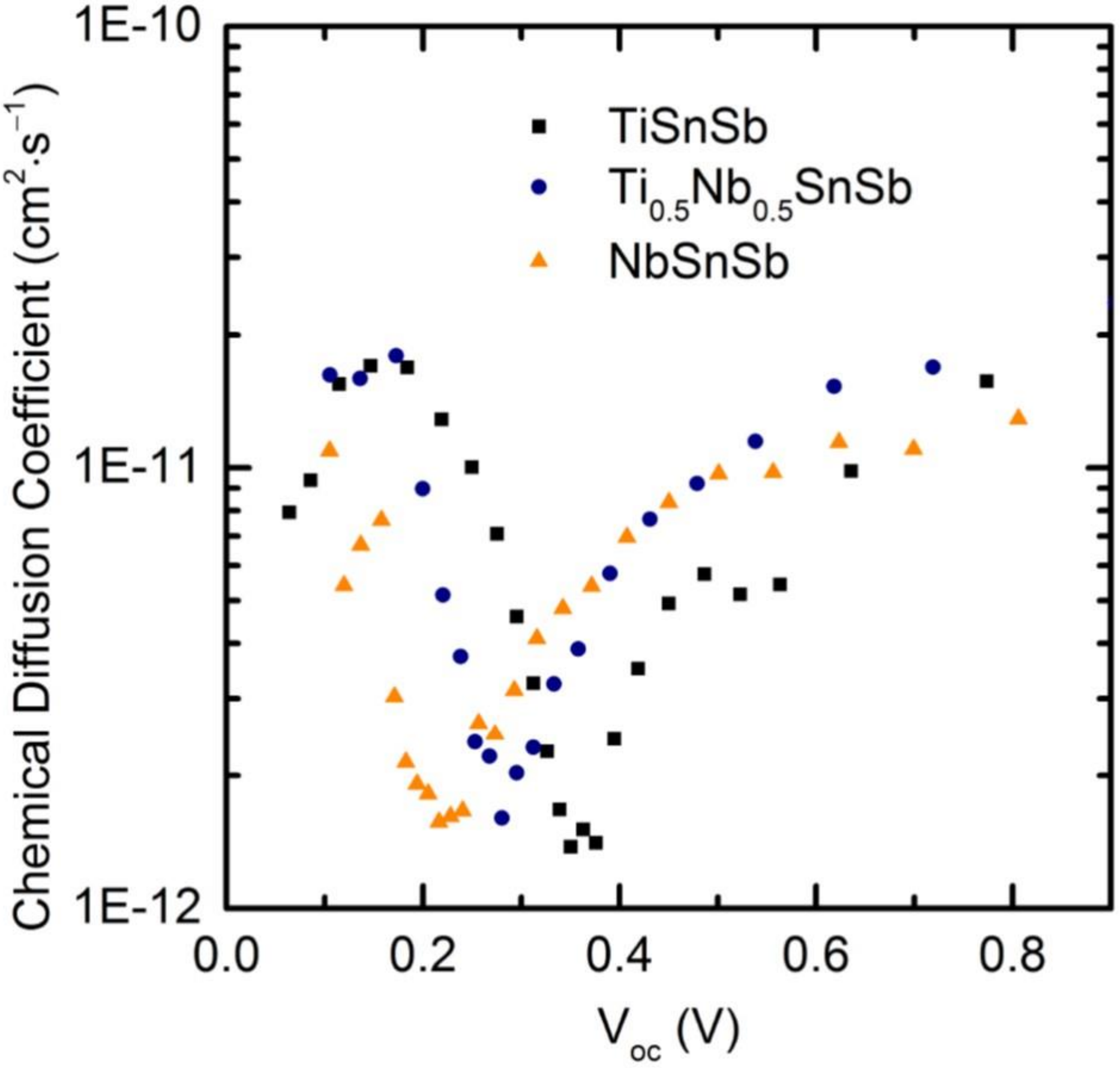

Figure 7 : $\widetilde{D}_{Li}$ as a function of potential for MSnSb (M = Ti, $Ti_{0.5}Nb_{0.5}$, Nb) from coulometric titration. In each alloy, lithium diffusion varies by an order of magnitude as a function of potential. The series exhibits systematic composition dependence; electroinactive Nb shifts the diffusion minimum to lower potentials.

Supporting Information for

'Probing the role of the so-called inactive transition metal in conversion reactions : not so inactive!'

Table of Contents:

X-ray Absorption Spectroscopy

Ti K-edge X-ray absorption spectroscopy was used to follow the speciation of titanium during lithiation and the following charge of TiSnSb. The near-edge XAS (XANES) spectrum of the pristine sample, together with those recorded at the end of lithiation and the following delithiation, is shown in Figure S1. The spectrum of the lithiated sample is different from that of pristine TiSnSb, as expected from the transformation of the initial material during lithiation. However, the spectrum of lithiated TiSnSb does not reproduce the features typical of a Ti metal foil reference. For example, the peak at 4967 eV, typical for Ti metal, can only be hinted at in the spectrum of the lithiated sample. Nevertheless, it is known that metal nanoparticles produce spectra that are somewhat different from those of bulk metals [1], and it is therefore difficult to conclude on the formation of Ti nanoparticles based solely on the XANES spectrum. The spectrum of the delithiated electrode is very similar to that of the initial material, suggesting that delithiation produces a material that is chemically similar to pristince TiSnSb.

More information on the evolution of the chemical environment can be obtained by analysis of the extended fine structure of the XAS spectra (EXAFS). The EXAFS spectra of the samples analyzed are shown in Figure S2. As in the case of the XANES spectra, the EXAFS signals of both the pristine and the delithiated sample are very similar, suggesting a similar environment around the Ti centres during cycling. However, the spectrum of the lithiated samples is rather different: the main peak at 2.9 Å in the FT signal of pristine TiSnSb disappears and is replaced by a new peak centred at 2.2 Å in the lithiated sample.

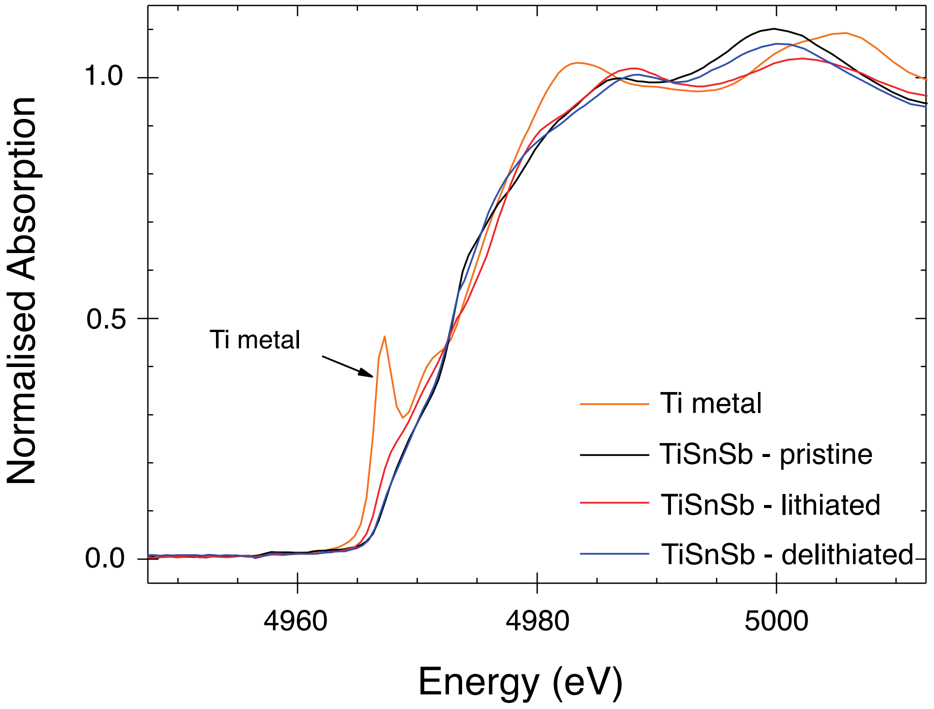

Figure S1: Ti K-edge XANES spectra for pristine TiSnSb and TiSnSb after full lithiation and delithiation. The spectrum of Ti metal foil is also shown for reference.

To gain further insight into the nature of the atoms surrounding the Ti centres, detailed fitting of the EXAFS spectra was performed and the parameters extracted (atomic distances, number of surrounding neighbours, Debye-Waller and amplitude reduction factor) are reported in Table S1. Based on the crystal structure of TiSnSb, 2 Ti nearest neighbours at 2.818 Å and 8 Sn and Sb neighbours distributed between 2.856 and 2.961 Å are expected in the spectrum of pristine TiSnSb. Additional Ti, Sn and Sb neighbours are observed above 4.76 Å, and are almost invisible in the FT signal.

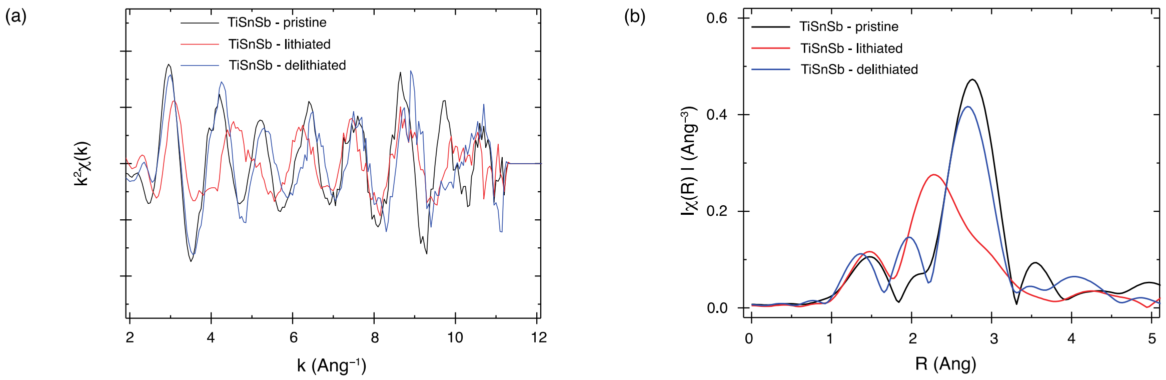

Figure S2: (a) EXAFS spectra and (b) corresponding envelope of the Fourier Transform (FT) of pristine TiSnSb and TiSnSb after full lithiation and delithiation. The FT signal is not phase corrected.

Considering that Sn and Sb are totally indistinguishable in the EXAFS analysis, because of their very similar atomic number, an acceptable fit is obtained using simply two shells: a first Ti-Ti shell accounting for 2 Ti neighbours, and a second shell comprising the 8 further Sn and Sb neighbours. The atomic distances (R) and Debye-Waller (σ^2) factors are in the expected ranges (Table S1). To fit the small contribution at 1.5 Å, a Ti-O shell that would account for the presence of a small TiO_2 impurity can be used. This is known to be present in the pristine material since a slight excess of Ti metal is usually employed during synthesis. The total value of the amplitude reduction factor, $S_0{}^2$, obtained by summing the contributions of TiSnSb and TiO_2 is 0.83, in the range typical of Ti K-edge EXAFS experiments.

Similar results are obtained using the same components to fit the sample of delithiated TiSnSb. In this case, only a slight, but significant, decrease of the Ti-Sn(Sb) bond length is observed, together with a small increase of the Debye-Waller factors, in line with a decrease in the crystallinity of the material.

Table S1: EXAFS parameters obtained during fitting of the spectra of pristine TiSnSb and TiSnSb after full lithiation and further delithiation where N is the number of neighbours in the considered shell, R is the atomic distances, σ^2 is Debye-Waller and S_0^2 is the amplitude reduction factor.

Sample	Shell	N	S_0^2	σ^2	R (Å)
Pristine TiSnSb	Ti-Ti	2	0.76(7)	0.011(6)	2.73(4)
	Ti-Sn(Sb)	8	0.76(7)	0.006(3)	2.85(2)
	Ti-O	6	0.07(3)	0.008(5)	2.00(4)
Lithiated TiSnSb	Ti-Ti	2	1.55(6)	0.010(6)	2.78(2)
	Ti-Sn(Sb)	8	0.11(7)	0.007(4)	2.85(4)
	Ti-O	6	0.06(2)	0.008(5)	1.98(4)
Delithiated TiSnSb	Ti-Ti	2	0.77(5)	0.010(6)	2.74(2)
	Ti-Sn(Sb)	8	0.82(6)	0.009(2)	2.79(2)
	Ti-O	6	0.07(2)	0.008(5)	1.98(4)

In contrast, differences are observed when the same parameters are used to fit the spectrum of lithiated TiSnSb. In this case, a strong increase in the intensity of the Ti-Ti contribution is observed, together with a strong decrease in the Ti-Sn(Sb) contribution. The value of S_0^2 obtained for the Ti-Ti shell (Table S1) has no physical meaning, since the amplitide reduction factor usually takes values around 0.8 and cannot exceed 1.0. However, this physical quantity is directly correlated to the number of nearest neighbours, and a high value of S_0^2 can be interpreted in terms of an underestimation of the number of nearest neighbours. Such a high value means that the number of nearest neighbours is more than twice the value of 2 used during the fit. This observation, together with a decrease in the Ti-Sn(Sb) contribution, is in line with the transformation of pristine TiSnSb into Ti-rich metal nanoparticles, probably surrounded by a Sn(Sb) rich environment. In hexagonal Ti metal, 12 Ti nearest neighbours are expected. However, a smaller value is usually observed in the case of nanoparticles, due to the lower coordination of surface atoms. These can be at the interface with Sn and Sb species, which would contribute to the observed Ti-Sn(Sb) shell, as already shown for the end of lithiation of $NiSb_2$ electrodes [1]. The observed increase in the Ti-Ti bond length, that moves towards the value usually observed for bulk Ti metal (2.87 Å), is further confirmation of the formation of Ti metal nanoparticles. It is noted that the Ti-O spectral contribution attributed to a TiO_2 impurity does not vary during delithiation and lithiation, thus not contributing to the electrochemistry.

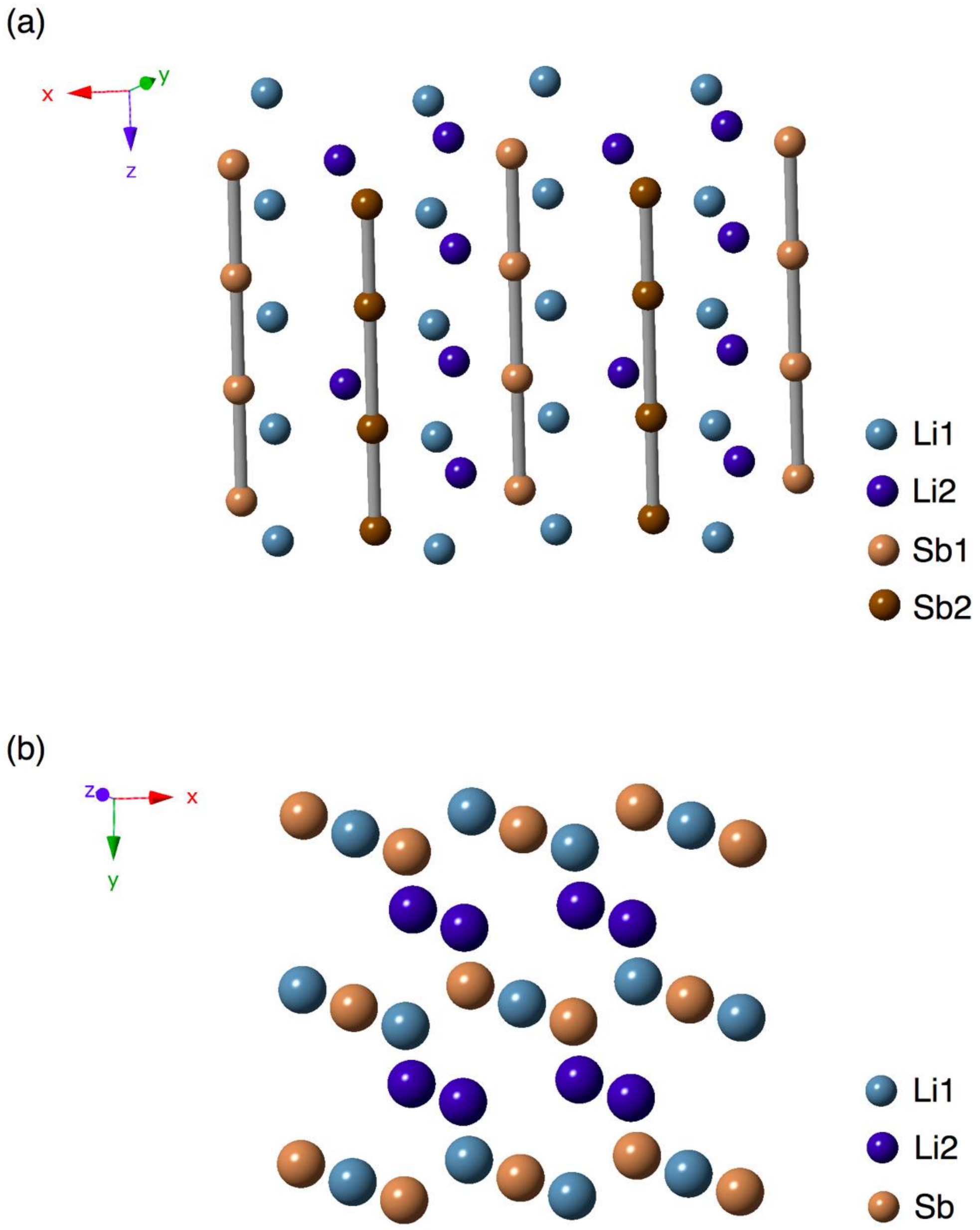

Figure S3: Crystal structures of (a) Li_2Sb (space group P-62m) and (b) Li_3Sb (space group Fm-3m).

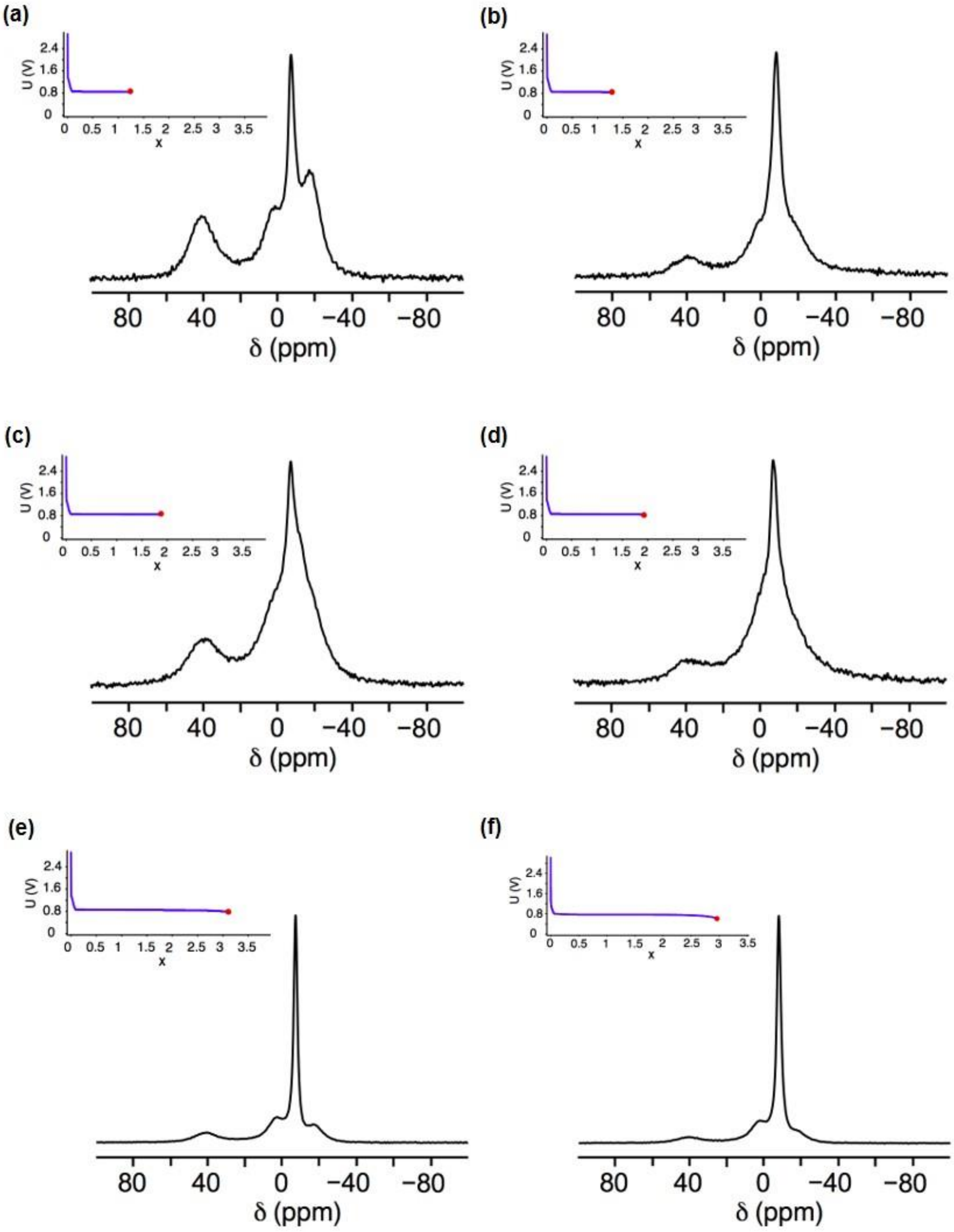

Figure S4: ^{7}Li (4.7 T) MAS NMR spectra obtained for Sb electrodes cycled (a,b) half way along the plateau at 0.8 V, (c,d) two thirds of the way along the plateau at 0.8 V and (e,f) to the end of the plateau at 0.8 V. In (a), (c) and (e) a cycling rate of C/2 was used and in (b), (d) and (f) a rate of 4C was used. The MAS rate was 25 kHz. In each the corresponding potential profiles are shown as insets.

The Lithiation of Sn and SnSb

The ^{7}Li NMR spectra obtained for samples of Sn at the end of lithiation are shown in Figures S5(a) and S6(a). The spectrum in Figure S5(a) has two broad resonances at 0 and 19 ppm and a smaller contribution at 32 ppm. Based on previous literature, the resonances are assigned to Li_7Sn_2, Li_7Sn_3 and LiSn, respectively [5]. The resonance at 0 ppm is extremely broad and is likely composed of multiple, overlapped phases that includes contributions from both the SEI and Li_7Sn_2. The presence of overlapped resonances makes it challenging to accurately identify all of the phases present. In contrast, the spectrum obtained for a sample cycled at 4C (Figure S6(a)) exhibits several distinct features at 78 ppm, 42 and 32 ppm, 16 ppm and 0 ppm, assigned to $Li_{22}Sn_5$, LiSn, $Li_{13}Sn_5$, Li_7Sn_3/SEI and Li_7Sn_2, respectively [5]. Again, it is challenging to accurately deconvolute the broad resonance at 0 ppm and identify the specific contributions from the SEI and the Sn-based phases. The resonance at 0 ppm is broad and likely contains contributions from multiple Sn-based phases, including Li_7Sn_2 and Li_5Sn_2. However, with no distinct features it is difficult to confirm the quantity of each phase present. ^{7}Li NMR spectra obtained after a relaxation period (the blue spectra in Figures S5(a) and S6(a)) indicate that the Sn phases formed at the end of lithiation are stable with time, as very little evolution is observed.

Both Sn and Sb are electrochemically active to Li, therefore a mixture of Li-Sn and Li-Sb phases are expected to form during the lithiation of SnSb [5-7].

Samples of SnSb were cycled at rates of C/2 and 4C to the end of lithiation (10 mV) and the corresponding ^{7}Li NMR spectra are shown in Figures S5(b) and S6(b), respectively. In both cases, a single broad resonance is observed with very few distinct features. It is likely that a complex mix of Li-Sn and Li-Sb phases is formed that includes Li_3Sb, Li_7Sn_2, Li_7Sn_3 $Li_{13}Sn_5$, $Li_{22}Sn_5$ and LiSn, as well as a contribution from the SEI. It is, however, challenging to accurately assign the Sn- and Sb-based phases formed in each case, as very few distinct features are observed. Moreover, there are no distinct plateaus or features in the corresponding electrochemical data that can assist in distinguishing the different stages of lithiation. A resonance is observed at 42 ppm in the spectrum obtained for the sample cycled at C/2, indicating the presence of LiSn [5]. It is noted that no distinct resonances are observed at negative chemical shifts (specifically −8.8 ppm) where, based on our earlier electrochemical and mechanosynthesis studies, the isolated bulk phase Li_3Sb is expected to occur. It is likely that the presence of Sn is influencing the local Li environments and the Li-Sn and Li-Sb phases formed are interacting with one another. During the lithiation process, a conversion reaction takes place, which destroys the initial rocksalt structure of SnSb. Hence, as in the case of TiSnSb, the Li_3Sb formed at the end of lithiation will have a much smaller particle size when compared to Li_3Sb produced via conventional ball milling or electrochemical techniques [2-3]. Such differences will be translated in the corresponding ^{7}Li NMR parameters, in particular the chemical shift. Spectra were acquired after a relaxation period and, in both cases, no evolution was observed, suggesting that the phases formed are stable with time. The presence of a single resonance is in agreement with the work of Fernández-Madrigal *et al.* [4]. The capacity we obtained at the end of lithiation for SnSb corresponds to 7 Li per SnSb formula unit, while in reference 4 the reaction of 10 Li per formula unit seems to be reached. Such a difference could be due to different electrode formulation or cycling conditions. Nevertheless, the reaction of 7 Li in reference 4 corresponds to a potential of 0.3 V, for which no negative ^{7}Li NMR shift can be observed.

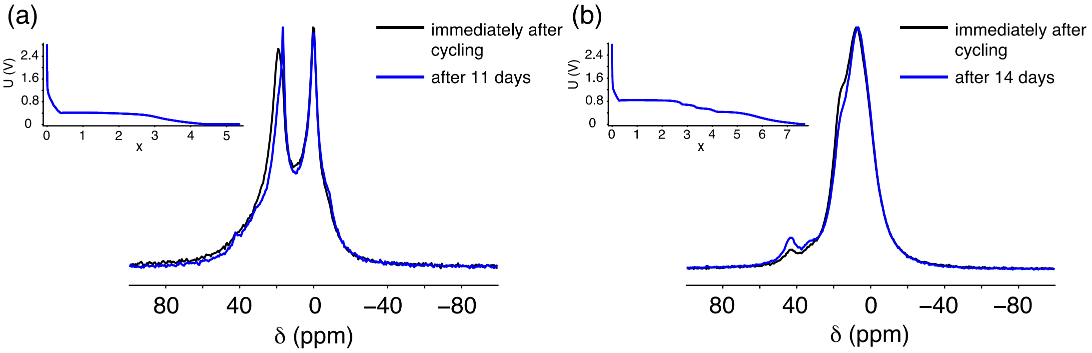

Figure S5: ^{7}Li (4.7 T) MAS NMR spectra obtained after electrochemical cycling of (a) pure Sn and (b) SnSb. All samples were cycled at a rate of C/2. In each case, spectra obtained immediately after reaching the end of lithiation are shown in black and spectra obtained after an additional relaxation period are in blue. The MAS rate was 25 kHz. Also shown as insets are the potential profiles obtained for each.

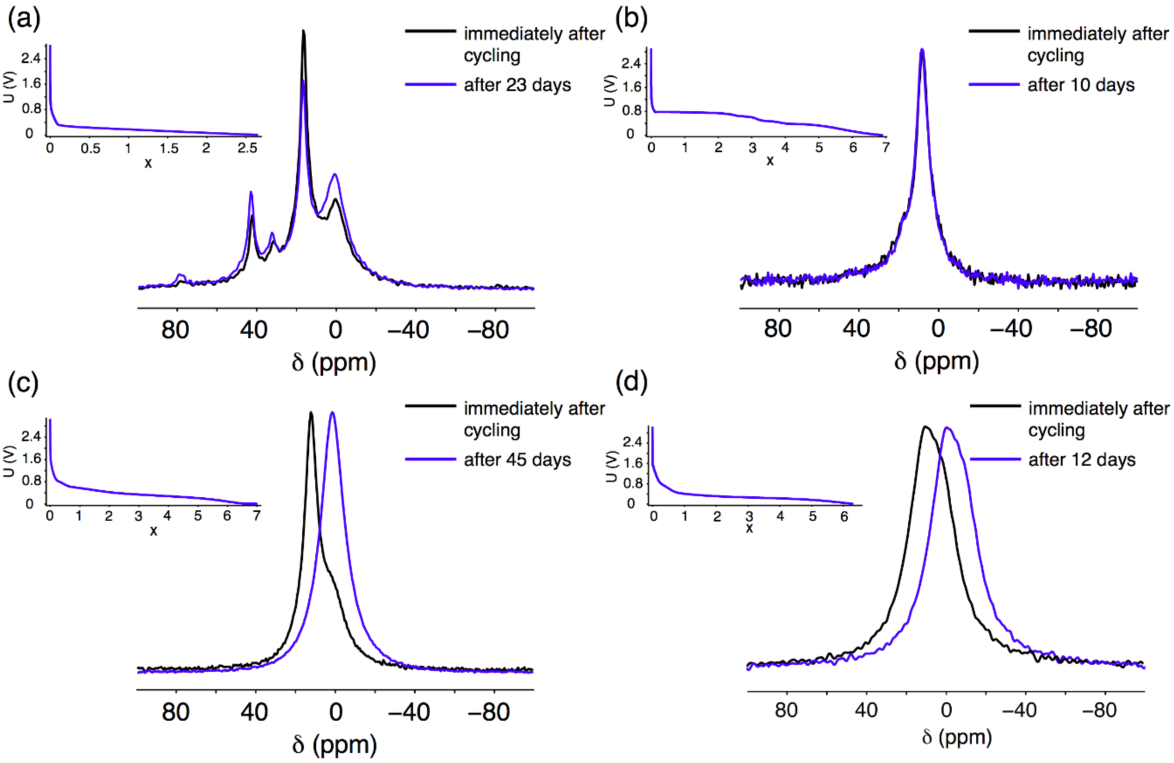

Figure S6: ^{7}Li (4.7 T) MAS NMR spectra obtained after electrochemical cycling of (a) pure Sn, (b) SnSb, (c) $TiSb_2$ and (d) $NbSb_2$. All samples were cycled at a rate of 4C. In each case, spectra obtained immediately after reaching the end of lithiation are shown in black and spectra obtained after an additional relaxation period are in blue. The MAS rate was 25 kHz. Also shown as insets in each case are the potential profiles obtained for each.

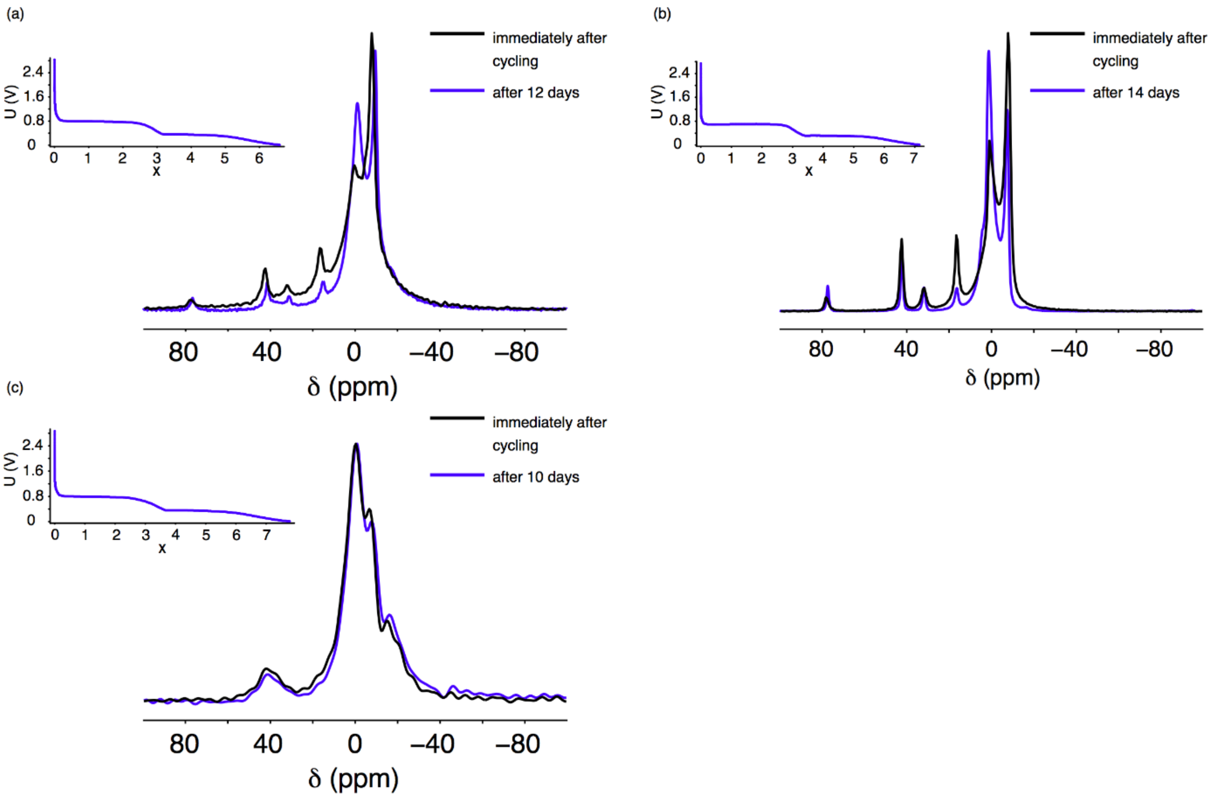

Figure S7: ^{7}Li (4.7 T) MAS NMR spectra ontained after electrochemical cycling of composites (a) M1, (b) M2 and (c) M3. All samples were cycled at 4C. In each case, spectra obtained immediately after reaching the end of lithiation are shown in black and spectra obtained after an additional relaxation period are in blue. The MAS rate was 25 kHz. Also shown as insets are the potential profiles obtained for each.

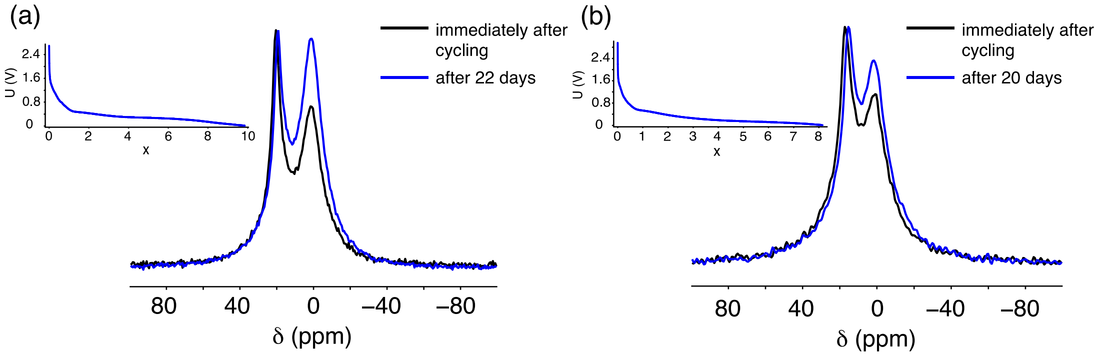

Figure S8: ^{7}Li (4.7 T) MAS NMR spectra obtained immediately after electrochemical cycling to the end of lithiation (black) for (a) TiSnSb and (b) NbSnSb. Both samples were cycled at a rate of C/2. The corresponding potential profiles are displayed as insets. Spectra obtained after an additional relaxation period are shown in blue. The MAS rate was 25 kHz.

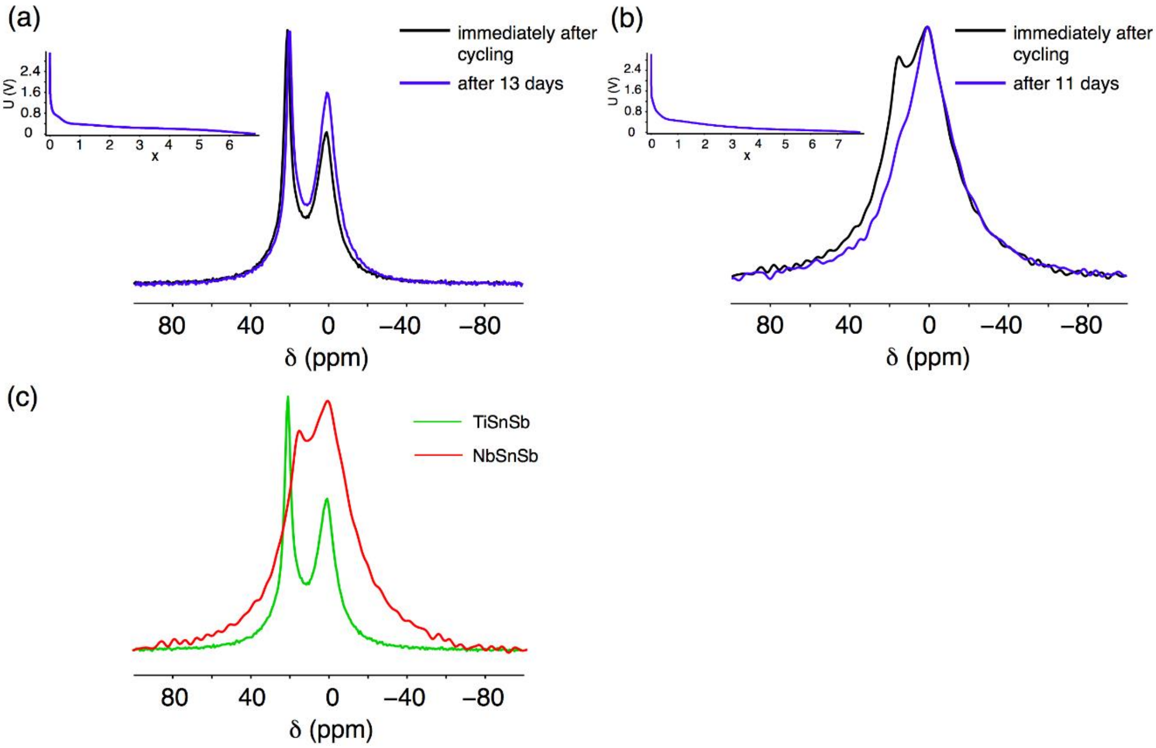

Figure S9: ^{7}Li (4.7 T) MAS NMR spectra obtained immediately after electrochemical cycling to the end of lithiation for (a) TiSnSb and (b) NbSnSb. Also shown in (c) for comparison is an overlay of the two spectra. Both samples were cycled at a rate of 4C. The corresponding potential profiles are displayed as insets in (a) and (b). Spectra obtained after an additional relaxation period are shown in blue. The MAS rate was 25 kHz.

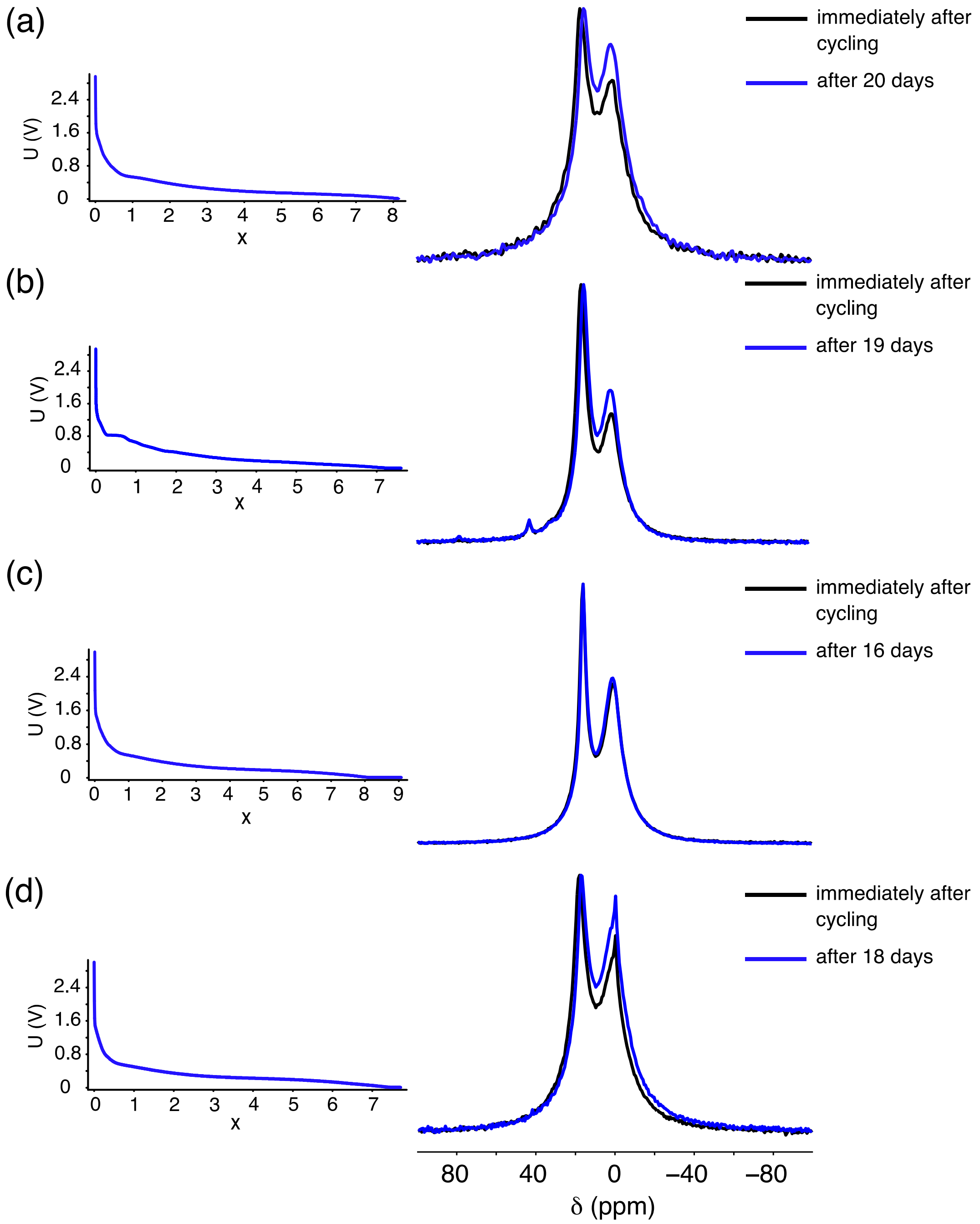

Figure S10: ^{7}Li (4.7 T) MAS NMR spectra obtained after electrochemical cycling to the end of lithiation for (a) NbSnSb, (b) $Ti_{0.25}Nb_{0.75}SnSb$, (c) $Ti_{0.5}Nb_{0.5}SnSb$ and (d) $Ti_{0.75}Nb_{0.25}SnSb$. All samples were cycled at a rate of C/2. Also shown are the corresponding potential profiles. Spectra obtained immediately after reaching the end of lithiation are shown in black and those obtained after an additional relaxation period are shown in blue. The MAS rate was 25 kHz.

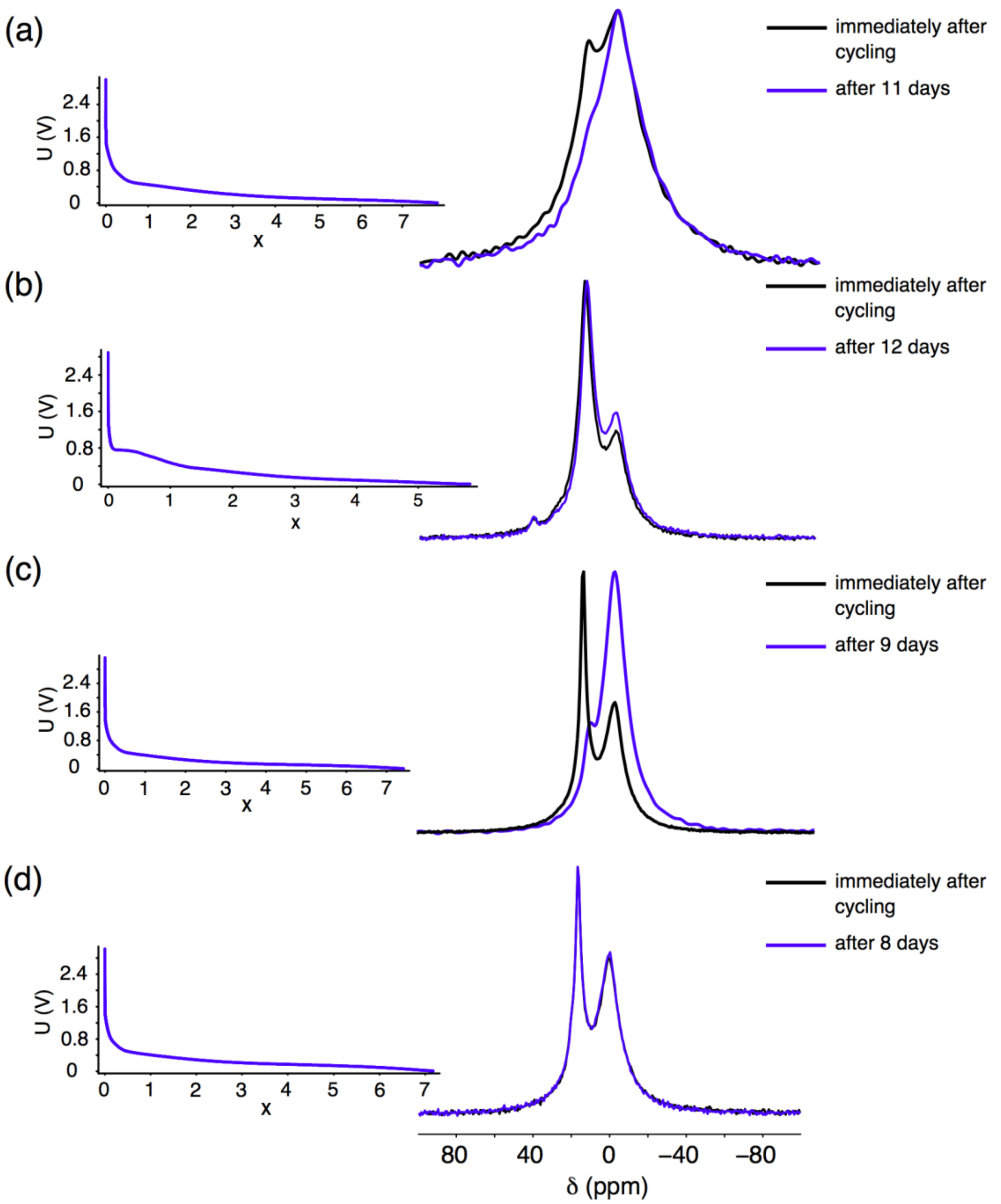

Figure S11: ^{7}Li (4.7 T) MAS NMR spectra obtained after electrochemical cycling to the end of lithiation for (a) NbSnSb, (b) $Ti_{0.25}Nb_{0.75}SnSb$, (c) $Ti_{0.5}Nb_{0.5}SnSb$ and (d) $Ti_{0.75}Nb_{0.25}SnSb$. All samples were cycled at a rate of 4C. Also shown are the corresponding potential profiles. Spectra obtained immediately after reaching the end of lithiation are shown in black and those obtained after an additional relaxation period are shown in blue. The MAS rate was 25 kHz.

References:

[1] C. Marino, B. Fraisse, M. Womes, C. Villevieille, L. Monconduit, L. Stievano, At the Heart of a Conversion Reaction: An Operando X-ray Absorption Spectroscopy Investigation of $NiSb_2$, a Negative Electrode Material for Li-ion Batteries, J. Phys. Chem. C 118 (2014) 27772-27780.

[2] M.T.Sougrati, J. Fullenwarth, A. Debenedetti, B. Fraisse, J.C. Jumas, L. Monconduit, TiSnSb a new efficient negative electrode for Li-ion batteries: mechanism investigations by *operando*-XRD and Mössbauer techniques, J. Mater. Chem. 21 (2011) 10069-10076.

[3] C. Marino, M.T.Sougrati, B. Gerke, R. Pöttgen, H. Huo, M. Ménétrier, C.P. Grey, L. Monconduit, Role of Structure and Interfaces in the Performance of TiSnSb as an Electrode for Li-Ion Batteries, Chem. Mater. 24 (2012) 4735-4743.

[4] F.J. Fernández-Madrigal, P. Lavela, C.P. Vicente, J.L.Tirado, X-ray diffraction, ^{7}Li MAS NMR spectroscopy and ^{119}Mössbauer spectroscopy study of SnSb-based electrode materials, Chem. Mater. 14(2002) 2962-2968.

[5] E. Bekaert, F. Robert, P.E. Lippens, M. Ménétrier, ^{7}Li NMR knight shifts in Li-Sn compounds: MAS NMR measurements and correlation with DFT calculations, J. Phys. Chem. C 114 (2010) 6749-6754.

[6] J. O. Besenhard, M. Wachtler, M. Winter, R. Andreaus, I. Rom, W. Sitte, Kinetics of Li insertion into polycrystalline and nanocrystalline 'SnSb' alloys investigated by transient and steady state techniques, J. Power Sources 81-82 (1999) 268-272.

[7] M. Winter, J.O. Besenhard, Electrochemical lithiation of tin and tin-based intermetallics and composites, Electrochim. Acta 45(1999) 31-50.

Citation on deposit: Johnston, K. E., Darwiche, A., Stievano, L., Griffith, K. J., Dupré, N., Grey, C. P., & Monconduit, L. (2024). Probing the role of the so-called inactive transition metal in conversion reactions: not so inactive!. Energy Storage Materials, 71, Article 103586. https://doi.org/10.1016/j.ensm.2024.103586